NASA TECHNICAL NOTE

NASA TN D-7721

NASA TN D-7721

WIND-TUNNEL INVESTIGATION TO DETERMINE THE LOW-SPEED YAWING STABILITY DERIVATIVES OF A TWIN-JET FIGHTER MODEL AT HIGH ANGLES OF ATTACK

by Paul L. Coe, Jr., and William A. Newsom, Jr.

Langley Research Center
Hampton, Va. 23665

NATIONAL AERONAUTICS AND SPACE ADMINISTRATION • WASHINGTON, D. C. • AUGUST 1974

1. Report No.	2. Government Accession No.	3. Recipient's Catalog No.
NASA TN D-7721		

4. Title and Subtitle	5. Report Date
WIND-TUNNEL INVESTIGATION TO DETERMINE THE LOW-SPEED YAWING STABILITY DERIVATIVES OF A TWIN-JET FIGHTER MODEL AT HIGH ANGLES OF ATTACK	August 1974
	6. Performing Organization Code
7. Author(s)	8. Performing Organization Report No.
Paul L. Coe, Jr., and William A. Newsom, Jr.	L-9664
	10. Work Unit No.
9. Performing Organization Name and Address	501-26-04-02
NASA Langley Research Center Hampton, Va. 23665	11. Contract or Grant No.
	13. Type of Report and Period Covered
12. Sponsoring Agency Name and Address	Technical Note
National Aeronautics and Space Administration Washington, D.C. 20546	14. Sponsoring Agency Code

15. Supplementary Notes

16. Abstract

An investigation was conducted to determine the low-speed yawing stability derivatives of a twin-jet fighter airplane model at high angles of attack. Tests were performed in a low-speed tunnel utilizing variable-curvature walls to simulate pure yawing motion.

The results of the study showed that at angles of attack below the stall the yawing derivatives were essentially independent of the yawing velocity and sideslip angle. However, at angles of attack above the stall some nonlinear variations were present and the derivatives were strongly dependent upon sideslip angle. The results also showed that the rolling moment due to yawing C_{l_r} was primarily due to the wing-fuselage combination, and that at angles of attack below the stall both the vertical and horizontal tails produced significant contributions to the damping in yaw C_{n_r}. Additionally, the tests showed that the use of the forced-oscillation data to represent the yawing stability derivatives is questionable, at high angles of attack, due to large effects arising from the acceleration in sideslip derivatives.

17. Key Words (Suggested by Author(s))	18. Distribution Statement
Yawing derivatives Acceleration in sideslip derivatives High angles of attack F-4 Phantom jet model	Unclassified – Unlimited STAR Category 02

19. Security Classif. (of this report)	20. Security Classif. (of this page)	21. No. of Pages	22. Price*
Unclassified	Unclassified	39	$3.25

*For sale by the National Technical Information Service, Springfield, Virginia 22151

WIND-TUNNEL INVESTIGATION TO DETERMINE THE LOW-SPEED YAWING STABILITY DERIVATIVES OF A TWIN-JET FIGHTER MODEL AT HIGH ANGLES OF ATTACK

By Paul L. Coe, Jr., and William A. Newsom, Jr.
Langley Research Center

SUMMARY

An investigation was conducted to determine the low-speed yawing stability derivatives of a twin-jet fighter airplane model at high angles of attack. Tests were performed in a low-speed tunnel utilizing variable-curvature walls to simulate pure yawing motion.

The results of the study showed that at angles of attack below the stall the yawing derivatives were essentially independent of the yawing velocity and sideslip angle. However, at angles of attack above the stall some nonlinear variations were present and the derivatives were strongly dependent upon sideslip angle. The results also showed that the rolling moment due to yawing C_{l_r} was primarily due to the wing-fuselage combination, and that at angles of attack below the stall both the vertical and horizontal tails produced significant contributions to the damping in yaw C_{n_r}. Additionally, the tests showed that the use of the forced-oscillation data to represent the yawing stability derivatives is questionable, at high angles of attack, due to large effects arising from the acceleration in sideslip derivatives.

INTRODUCTION

The National Aeronautics and Space Administration is currently engaged in a broad research program designed to supply fundamental information in the areas of automatic spin prevention, inherent spin resistance, and development of theoretical techniques for stall/spin studies. A major requirement for such a research program is an understanding of aerodynamic phenomena at high angles of attack, including techniques for the measurement of these characteristics.

Previous wind-tunnel studies of swept wings (refs. 1 to 4) have shown that the classical dynamic stability derivatives of swept wings at high angles of attack require specialized test techniques in order to identify derivatives due to pure angular rates (such as rolling and yawing velocities) and derivatives due to linear accelerations (such as rate of change of sideslip). The present investigation was conducted in order to determine

the dynamic yawing stability derivatives of a contemporary fighter-airplane configuration at high angles of attack. The tests were conducted in a curved-flow wind tunnel which permitted the simulation of pure yawing motion rather than the combined yawing and sideslipping motion normally produced by other dynamic test techniques, such as the forced-oscillation test technique described in reference 5. The results of the present tests are compared with the results of forced-oscillation tests previously conducted at the Langley Research Center (see ref. 6) in which the same model was used.

SYMBOLS

All aerodynamic data are presented with respect to the stability system of axes as shown in figure 1. Moment data are presented with respect to a center-of-gravity position of 33 percent of the wing mean aerodynamic chord. Measurements and calculations were made in U.S. Customary Units and are presented herein in the International System of Units (SI) with equivalent values given parenthetically in the U.S. Customary Units.

b	wing span, m (ft)
$\bar{c}$	wing mean aerodynamic chord, m (ft)
$\bar{c}_t$	horizontal-tail mean aerodynamic chord, m (ft)
C_D	drag coefficient, F_D/qS
C_L	lift coefficient, F_L/qS
C_l	rolling-moment coefficient, M_X/qSb
C_m	pitching-moment coefficient, $M_Y/qS\bar{c}$
C_n	yawing-moment coefficient, M_Z/qSb
C_Y	side-force coefficient, F_Y/qS
F_D	drag force, N (lb)
F_L	lift force, N (lb)
F_Y	side force, N (lb)

M_X rolling moment, m-N (ft-lb)

M_Y pitching moment, m-N (ft-lb)

M_Z yawing moment, m-N (ft-lb)

q free-stream dynamic pressure, N/m^2 (lb/ft^2)

r yawing velocity, rad/sec

$\frac{rb}{2V}$ nondimensional yawing-velocity parameter

S wing area, m^2 (ft^2)

V free-stream velocity, m/sec (ft/sec)

X,Y,Z stability axes (fig. 1)

α angle of attack, deg

β angle of sideslip, deg

$\dot{\beta}$ rate of change of sideslip angle, rad/sec

$$C_{l_\beta} = \frac{\partial C_l}{\partial \beta} \qquad C_{n_\beta} = \frac{\partial C_n}{\partial \beta} \qquad C_{Y_\beta} = \frac{\partial C_Y}{\partial \beta}$$

$$C_{l_{\dot{\beta}}} = \frac{\partial C_l}{\partial \frac{\dot{\beta} b}{2V}} \qquad C_{n_{\dot{\beta}}} = \frac{\partial C_n}{\partial \frac{\dot{\beta} b}{2V}} \qquad C_{Y_{\dot{\beta}}} = \frac{\partial C_Y}{\partial \frac{\dot{\beta} b}{2V}}$$

$$C_{l_r} = \frac{\partial C_l}{\partial \frac{rb}{2V}} \qquad C_{n_r} = \frac{\partial C_n}{\partial \frac{rb}{2V}} \qquad C_{Y_r} = \frac{\partial C_Y}{\partial \frac{rb}{2V}}$$

Model component designations:

F fuselage

H horizontal tail

V vertical tail

W wing

MODEL AND APPARATUS

Model

The investigation was conducted by using a 0.0915-scale model of a twin-jet fighter airplane. The model was primarily of fiber-glass construction with blocked inlets. A three-view sketch of the model is presented in figure 2, and pertinent dimensional characteristics of the full-scale airplane are given in table I.

Wind Tunnel

The data presented herein were obtained in a low-speed tunnel (previously known as the Langley stability tunnel) which has a 1.83- by 1.83-m (6- by 6-ft) curved-flow test section. The tunnel was acquired by the Virginia Polytechnic Institute in 1958 and is currently operated at that institute. The tunnel is used with a straight test section to obtain conventional static test data. The tunnel also has a unique capability in that the vertical sidewalls of the test section are designed with sufficient flexibility so that they may be deflected into a curve, thus creating a curved airflow past the model. Jackscrews are positioned at regular intervals along each wall to allow the curvature to be set at prescribed values.

In order to simulate flight in a curved path it is also necessary to redistribute the velocity profile in the radial direction. This is accomplished by installing vertical wire screens in the flow upstream of the test section. These screens vary in mesh across the wind tunnel, with the densest portion of the screens located nearer the center of curvature. A sketch showing a typical curved-flow test arrangement is shown in figure 3. A complete description of the tunnel and its operation is given in reference 7.

TESTS AND CORRECTIONS

The force tests were conducted at a Reynolds number of approximately 0.73×10^6, based on the mean aerodynamic chord of the wing. Tests in both curved and straight flow were conducted for the fuselage-wing combination, the fuselage-wing—vertical-tail combination, and the complete model. The model was sting mounted, and measurements were made of the six force and moment components by using an internal strain-gage balance.

The tests were conducted over an angle-of-attack range from -10° to 45° for an angle-of-sideslip range from -10° to 10° in straight flow. For the curved-flow tests the angle-of-attack range was 0° to 45° for an angle-of-sideslip range from -5° to 5°. Three curvatures representing yawing flight to the left were selected for the curved-flow tests and resulted in values of the nondimensional yawing velocity $rb/2V$ of -0.0327, -0.0483, and -0.0637.

Experimentally determined blockage corrections have been applied to the data because of the relatively large size of the model in relation to the test-section area. Additionally, the side-force coefficients have been corrected to account for the radial pressure gradient in the tunnel in accordance with the method of reference 7.

RESULTS AND DISCUSSION

Results of Straight-Flow Static Tests

Longitudinal characteristics.- The variations of the static longitudinal aerodynamic characteristics of the model with angle of attack are shown in figure 4. These data show that the onset of wing stall occurred at approximately $\alpha = 15^{\circ}$, with a gradual well-defined stall at higher angles of attack.

Comparison of the data with and without the horizontal tail (fig. 4(a)) indicates that the horizontal tail remained effective in providing static longitudinal stability throughout the angle-of-attack range tested. Presented in figure 4(b) are data from reference 8 which were obtained with the same model at approximately the same value of Reynolds number, but in a 3.66- by 3.66-m (12- by 12-ft) octagonal test section of a low-speed wind tunnel at the Langley Research Center. The data are in relatively good agreement, but variations in C_m were noted at higher angles of attack. The close proximity of the horizontal tail to the tunnel floor in the present investigation probably contributed to the differences shown.

Lateral-directional characteristics.- The variation of the static lateral-directional characteristics of the model with angle of sideslip is presented in figure 5 for the various airframe component combinations tested. The data show that up to an angle of attack of 35° the variation of C_Y, C_n, and C_l with β is generally linear over a β range from -5° to 5°. When the β range was extended to -10° to 10°, the variation of C_Y, C_n, and C_l with β generally became nonlinear with the greatest nonlinearity at $\alpha = 20^{\circ}$.

The variation of static lateral-directional stability derivatives with angle of attack obtained over a range of sideslip angles from -5° to 5° is summarized for the various model components in figure 6. The data for the wing-fuselage combination, the wing-fuselage—vertical-tail combination, and the complete model show a loss of effective dihedral and a rapid decrease in directional stability at the stall.

As pointed out in reference 8, the loss of effective dihedral at the stall is associated with flow separation which causes reduced lift on the leading wing in a sideslipped condition. The analysis of reference 8 also shows that the factors producing the loss of directional stability at angles of attack near the stall are a loss of dynamic pressure at the vertical tail and an adverse sidewash field produced by flow separation on the wing-fuselage combination. As the angle of attack is increased above the stall, the vertical tail enters this adverse sidewash field which results in a complete loss of vertical-tail effectiveness as shown by the data of figure 6(a).

Shown in figure 6(b) is a comparison of the static lateral-directional derivatives as measured during the present study with those determined from the data of reference 6. Although the trends shown by the data are in fairly good agreement, some differences in the magnitudes of the derivatives occurred at high angles of attack.

Results of Curved-Flow Tests

Longitudinal characteristics.- The longitudinal aerodynamic characteristics of the model, obtained in the curved-flow tests, did not differ to any significant extent from the data in the straight-flow tests, and as a result the data are not presented herein.

Lateral-directional characteristics.- The variations of the static lateral-directional aerodynamic coefficients C_Y, C_n, and C_l with nondimensional yawing velocity $rb/2V$ at $\beta = 0^\circ$ and $\beta = \pm 5^\circ$ are presented for the fuselage-wing combination, the fuselage-wing—vertical-tail combination, and the complete configuration in figures 7, 8, and 9, respectively. These data are faired by using a least-squares linear curve fit. The variations of C_Y, C_n, and C_l with $rb/2V$ are shown to be relatively linear for angles of attack up to the onset of stall; however, as the angle of attack was increased above the stall some nonlinearities are noted.

The stability derivatives C_{Y_r}, C_{n_r}, and C_{l_r} obtained by using the least-squares linear curve fit over the range of nondimensional yawing velocities from 0 to -0.0637, for the data of figures 7 to 9, are summarized in figures 10 and 11.

Analysis of the data of figure 10 indicates that the magnitude of the rolling moment due to yawing derivative C_{l_r} was primarily due to the wing-body combination, since the horizontal and vertical tails provided only small changes in the value of the derivative from that for the wing-fuselage combination.

The variation of the damping-in-yaw derivative C_{n_r} with angle of attack shows that the complete model at $\beta = 0^\circ$ had stable values of damping in yaw (negative values of C_{n_r}) for angles of attack up to 27°. Unstable values of C_{n_r} were measured for the angle-of-attack range between 27° and 38°. The component tests indicate that the unstable values were caused by both instability of the wing-fuselage combination and reduced

effectiveness of the vertical tail. It is interesting to note that the contribution of the vertical tail to C_{n_r} appears to correlate with the trends shown by the tail contribution to C_{n_β} shown in figure 6(a).

Examination of figure 11 shows that yawing stability derivatives were essentially independent of β over the range of β from -5° to 5° up to the angle of attack at which stall occurred; however, at the higher angles of attack the derivatives appear to be strongly dependent upon sideslip.

Shown in figure 12 is a comparison of the yawing derivatives as measured during the present study with those obtained by using the forced-oscillation technique (amplitude, $\pm 5^\circ$; reduced frequency, 0.12) in reference 6. The large differences obtained by the two test techniques indicate a considerable need for individual measurements of the pure rate derivatives and the $\dot{\beta}$ derivatives if a valid aerodynamic description of this particular configuration is to be obtained in the high angle-of-attack range. It would be expected, for example, that large differences in dynamic stability characteristics might be obtained depending on the choice of derivatives used in the calculations.

SUMMARY OF RESULTS

An investigation to determine the yawing stability derivatives of a fighter airplane model has produced the following results:

1. At angles of attack below the stall the yawing derivatives were essentially independent of the yawing velocity and sideslip angle.

2. In the poststall angle-of-attack range some nonlinearity of the yawing characteristics with respect to yawing velocity was present, and the yawing derivatives were strongly dependent on sideslip angle.

3. The wing-fuselage combination was primarily responsible for the rolling moment due to yawing C_{l_r}.

4. At angles of attack below the stall both the vertical and horizontal tails provided large stabilizing increments to the damping-in-yaw parameter C_{n_r}.

5. The use of forced-oscillation data to represent the yawing stability derivatives, at high angles of attack, is questionable due to large effects arising from the acceleration in sideslip derivatives.

Langley Research Center
National Aeronautics and Space Administration,
Hampton, Va., July 8, 1974.

REFERENCES

1. Goodman, Alex; and Brewer, Jack D.: Investigation at Low Speeds of the Effect of Aspect Ratio and Sweep on Static and Yawing Stability Derivatives of Untapered Wings. NACA TN 1669, 1948.

2. Campbell, John P.; Johnson, Joseph L., Jr.; and Hewes, Donald E.: Low-Speed Study of the Effect of Frequency on the Stability Derivatives of Wings Oscillating in Yaw With Particular Reference to High Angle-of-Attack Conditions. NACA RM L55H05, 1955.

3. Letko, William; and Fletcher, Herman S.: Effects of Frequency and Amplitude on the Yawing Derivatives of Triangular, Swept, and Unswept Wings and of a Triangular-Wing-Fuselage Combination With and Without a Triangular Tail Performing Sinusoidal Yawing Oscillations. NACA TN 4390, 1958.

4. Lichtenstein, Jacob H.; and Williams, James L.: Low-Speed Investigation of the Effects of Frequency and Amplitude of Oscillation in Sideslip on the Lateral Stability Derivatives of a 60° Delta Wing, a 45° Sweptback Wing, and an Unswept Wing. NASA TN D-896, 1961. (Supersedes NACA RM L58B26.)

5. Hewes, Donald E.: Low-Subsonic Measurements of the Static and Oscillatory Lateral Stability Derivatives of a Sweptback-Wing Airplane Configuration at Angles of Attack From -10° to 90°. NASA MEMO 5-20-59L.

6. Anglin, Ernie L.; and Grafton, Sue B.: Results of Static and Dynamic Force Test of a 1/11-Scale Model of the F-4 Airplane and Their Applicability to Theoretical Spin Analysis – COORD NO. N-AM-147. NASA TM SX-2124, Naval Air System Command, 1970.

7. Bird, John D.; Jaquet, Byron M.; and Cowan, John W.: Effect of Fuselage and Tail Surfaces on Low-Speed Yawing Characteristics of a Swept-Wing Model as Determined in Curved-Flow Test Section of Langley Stability Tunnel. NACA TN 2483, 1951. (Supersedes NACA RM L8G13.)

8. Chambers, Joseph R.; and Anglin, Ernie L.: Analysis of Lateral-Directional Stability Characteristics of a Twin-Jet Fighter Airplane at High Angles of Attack. NASA TN D-5361, 1969.

TABLE I.- DIMENSIONAL CHARACTERISTICS OF FULL-SCALE AIRPLANE

Overall length	17.55 m (57.59 ft)
Wing:	
Span	11.71 m (38.41 ft)
Area (including leading-edge extension)	50.01 m^2 (538.34 ft^2)
Root chord	716.28 cm (282.00 in.)
Tip chord	119.38 cm (47.00 in.)
Mean aerodynamic chord, $\bar{c}$	488.95 cm (192.50 in.)
Longitudinal distance from leading edge of root chord to leading edge of $\bar{c}$	281.33 cm (110.76 in.)
Aspect ratio	2.74
Taper ratio	0.167
Sweepback of 25-percent-chord line	45.00^o
Dihedral (inboard of 69.5 percent b/2)	0^o
Dihedral (outboard of 69.5 percent b/2)	12.00^o
Incidence	1.00^o
Airfoil section:	
Root	Modified NACA 0006.4-64
Tip	Modified NACA 0003.0-64
Horizontal tail:	
Area (in chord plane)	8.80 m^2 (94.70 ft^2)
Movable area	7.19 m^2 (77.40 ft^2)
Span	5.40 m (17.705 ft)
Aspect ratio	3.31
Taper ratio	0.20
Sweepback of 25-percent-chord line	35.50^o
Dihedral	-23.00^o
Root chord (at airplane center line)	271.78 cm (107.00 in.)
Tip chord (theoretical)	54.36 cm (21.40 in.)
Airfoil section:	
Root (airplane center line)	Modified NACA 0003.7-64
Tip (theoretical)	Modified NACA 0003.0-64
Hinge-line location, percent $\bar{c}_t$	41.00
Vertical tail:	
Area	6.27 m^2 (67.50 ft^2)
Span	1.94 m (6.38 ft)
Taper ratio	0.227
Root chord	526.16 cm (207.15 in.)
Tip chord	119.63 cm (47.10 in.)
Sweepback of 25-percent-chord line	58.30^o
Airfoil section:	
Root	Modified NACA 0004.0-64
Tip	Modified NACA 0002.5-64

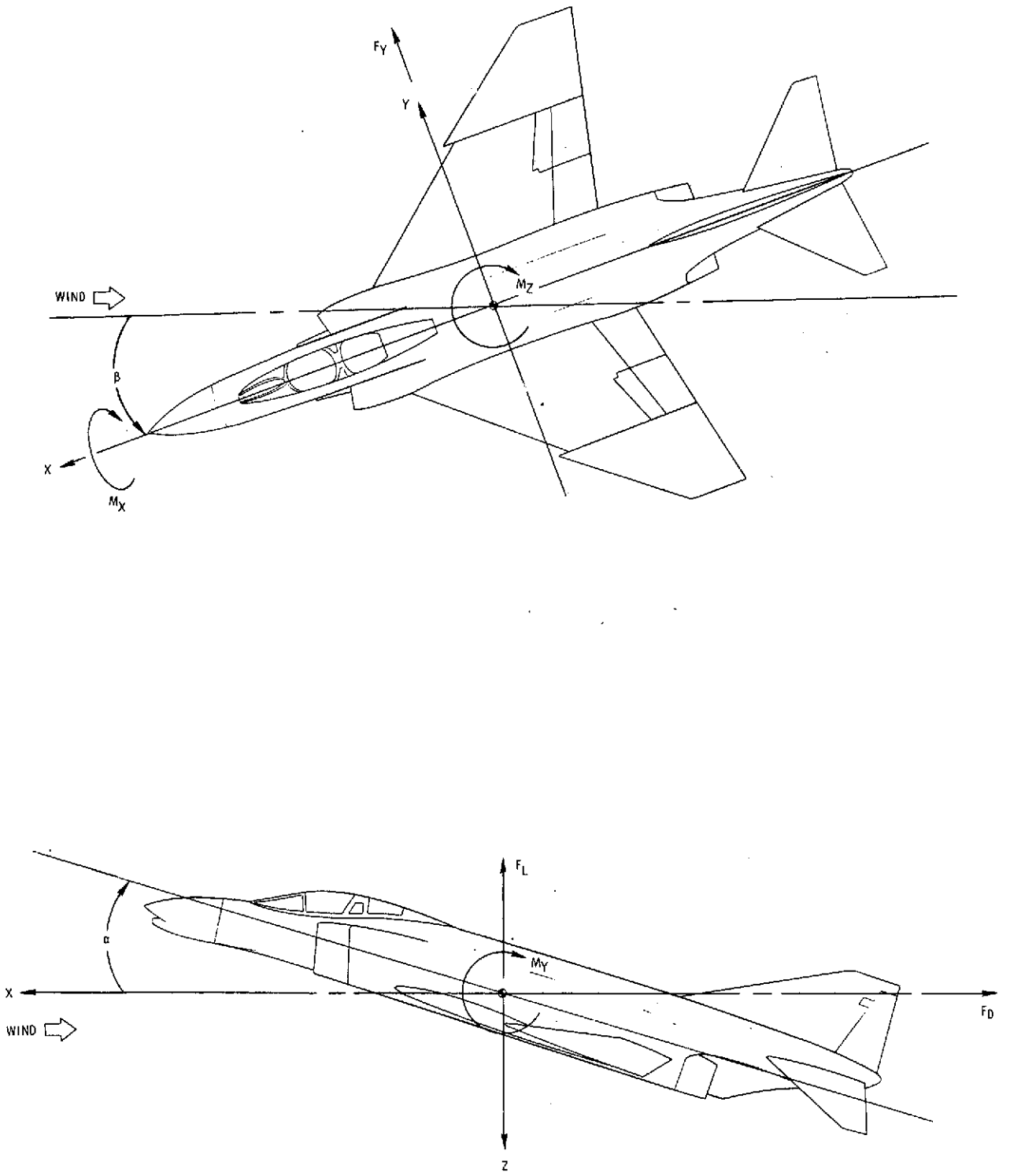

Figure 1.- Stability system of axes. Positive values of forces, moments, and angles are indicated by arrows.

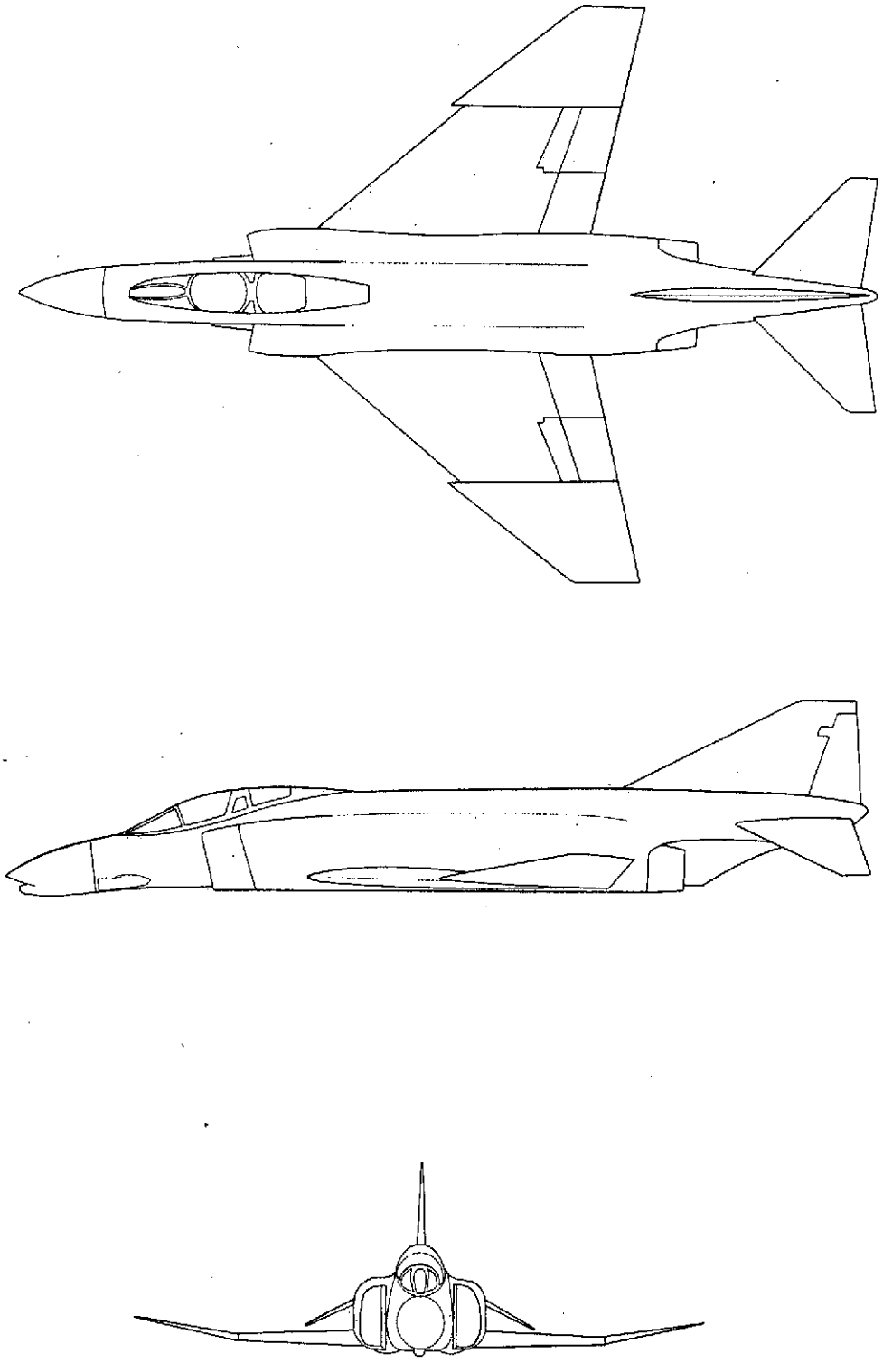

Figure 2.- Three-view sketch of airplane configuration.

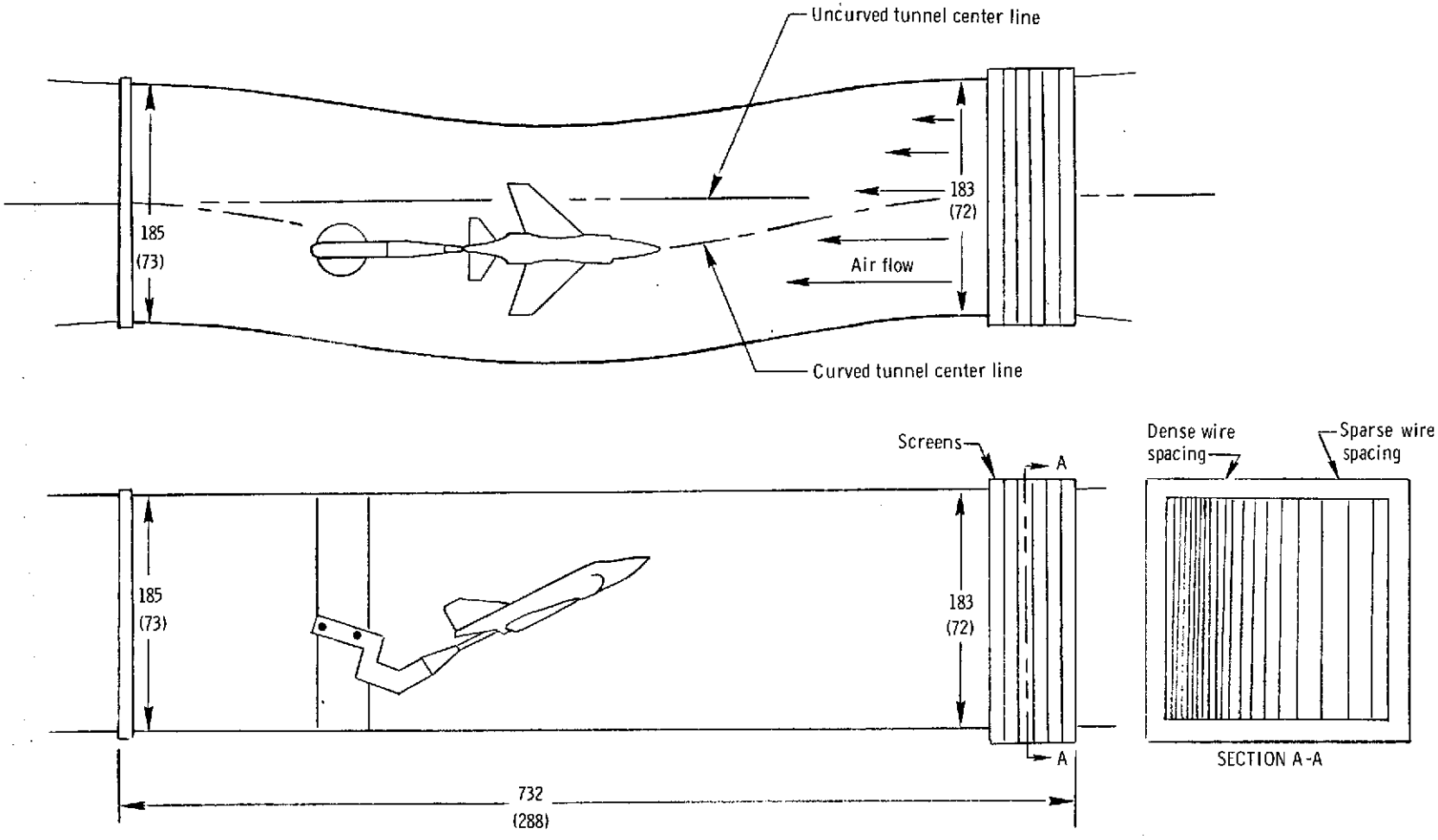

Figure 3.- Diagram of curved-flow test section of the wind tunnel. Dimensions are given in centimeters and parenthetically in inches.

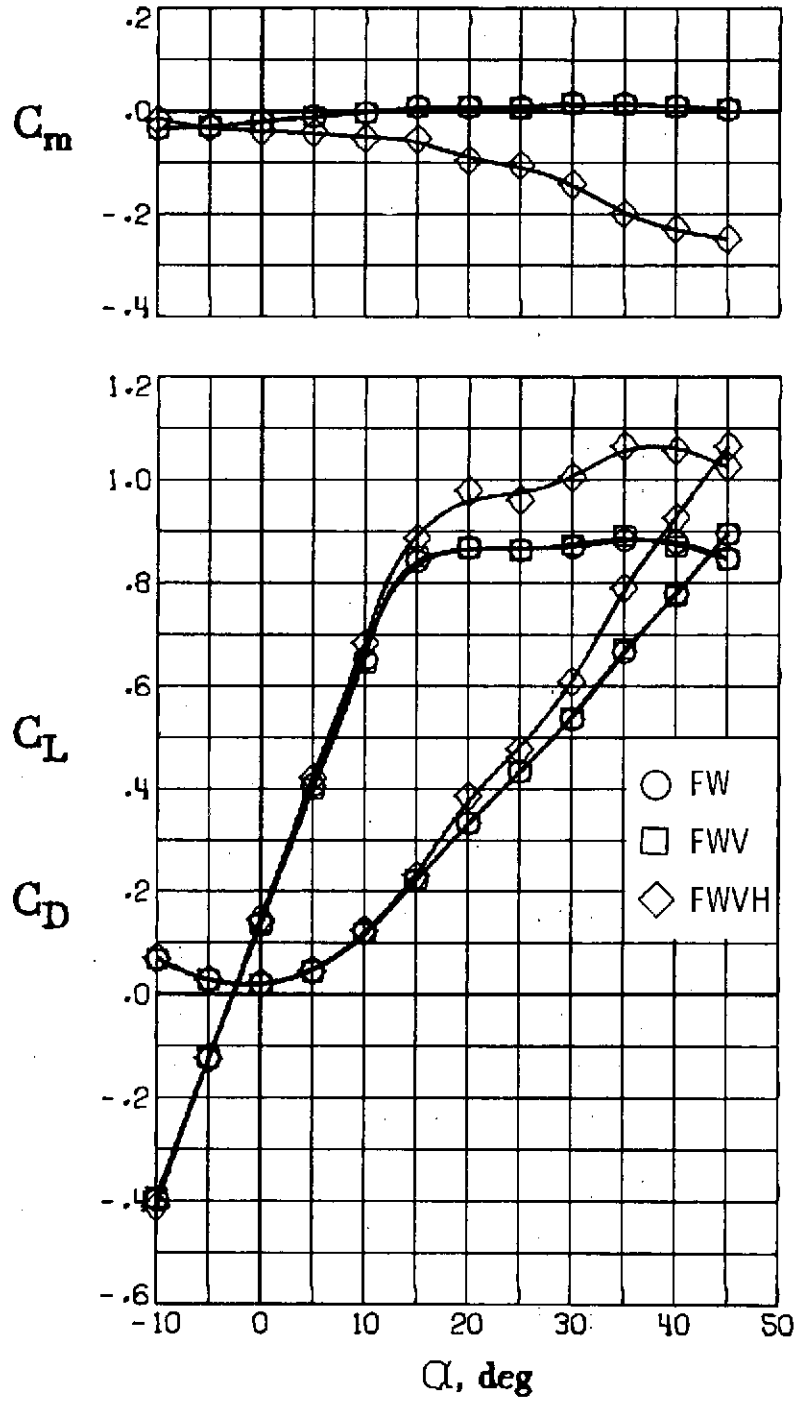

(a) Component buildup study.

Figure 4.- Variation of static longitudinal aerodynamic characteristics of model with angle of attack. $\beta = 0^{\circ}$.

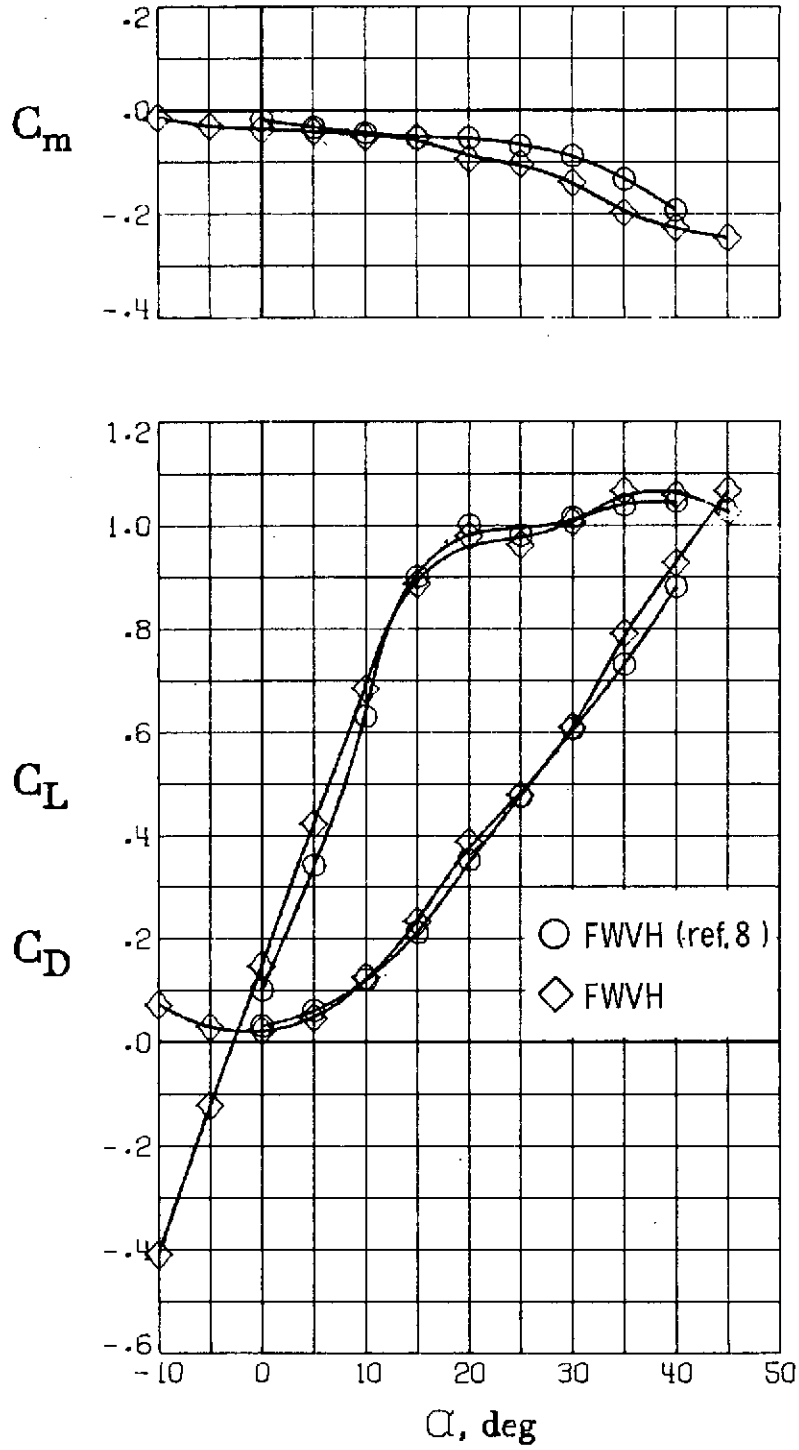

(b) Comparison of static longitudinal aerodynamic characteristics of present investigation with those of reference 8.

Figure 4.- Concluded.

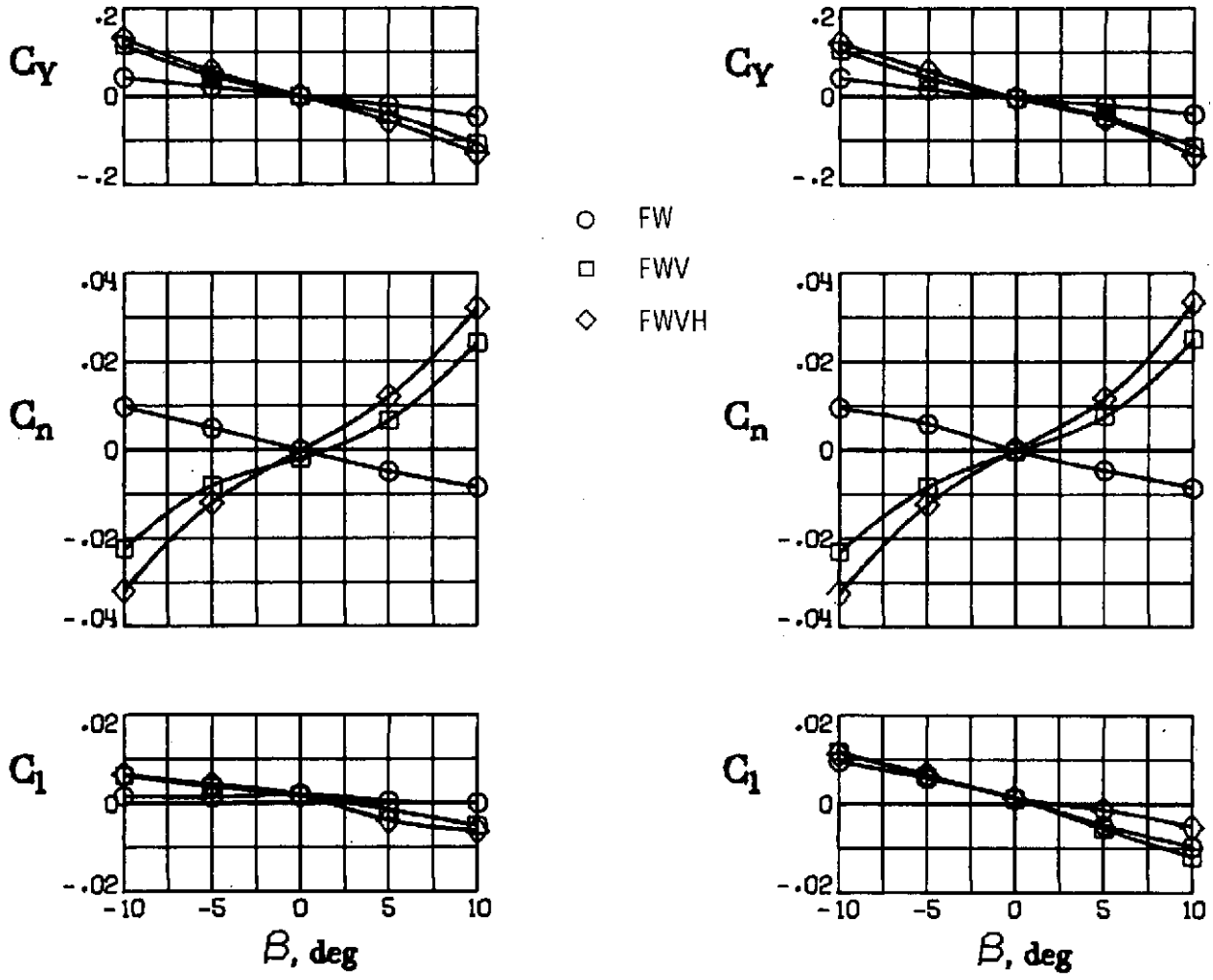

(a) $\alpha = 0^{\circ}$.

(b) $\alpha = 5^{\circ}$.

Figure 5.- Variation of static lateral-directional characteristics of model with angle of sideslip for various component combinations.

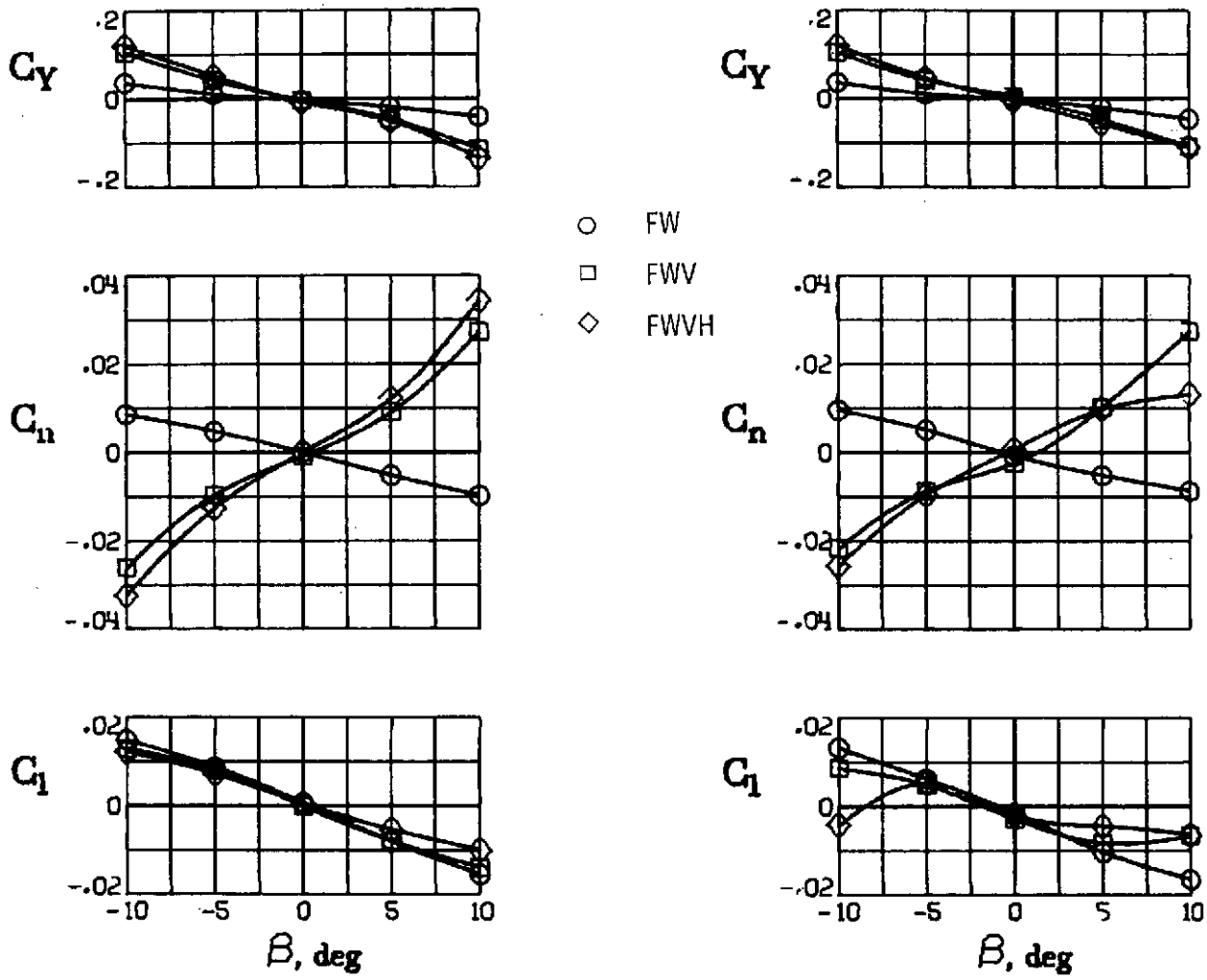

(c) $\alpha = 10^{\circ}$.

(d) $\alpha = 15^{\circ}$.

Figure 5.- Continued.

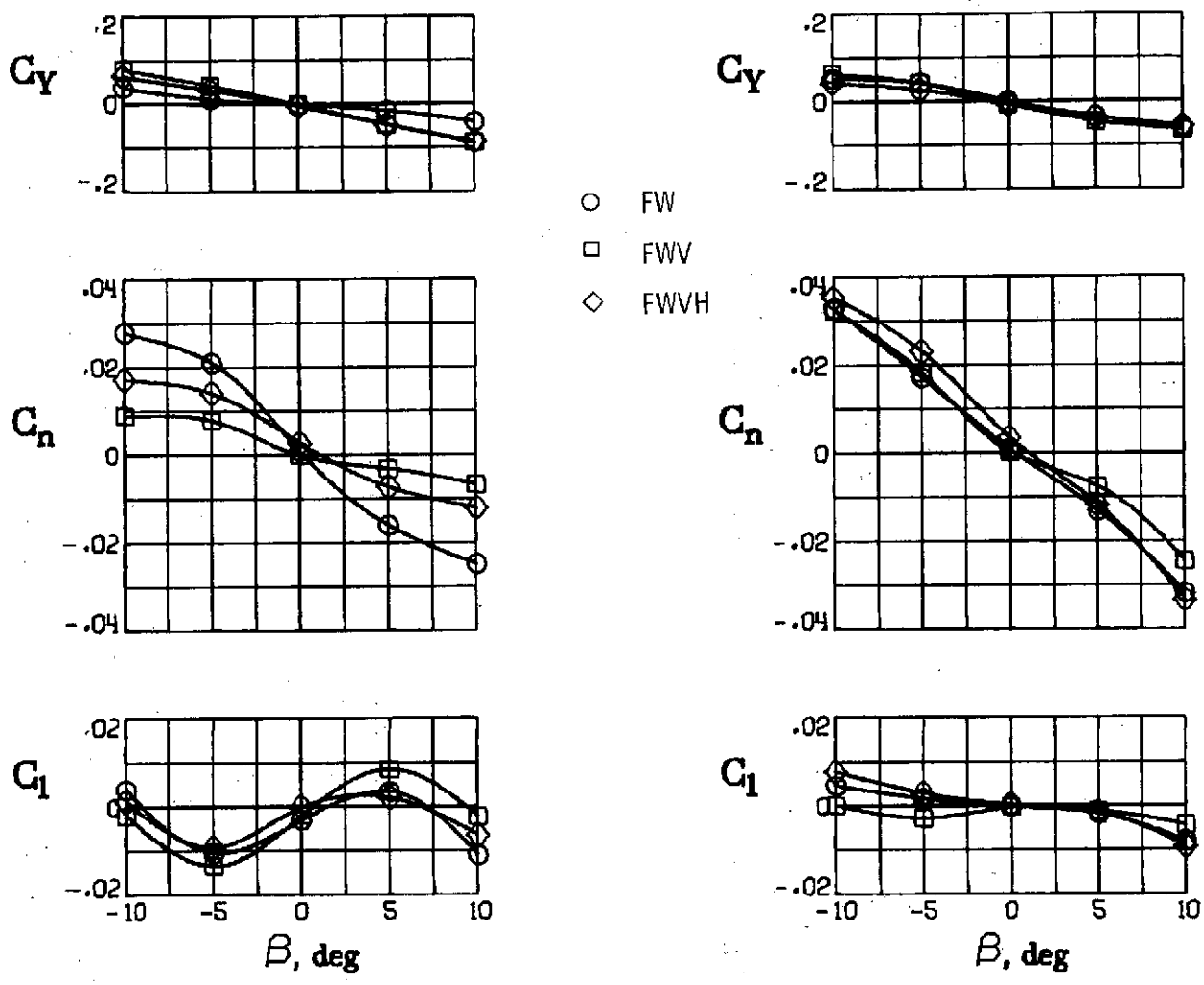

(e) $\alpha = 20^{\circ}$.

(f) $\alpha = 25^{\circ}$.

Figure 5.- Continued.

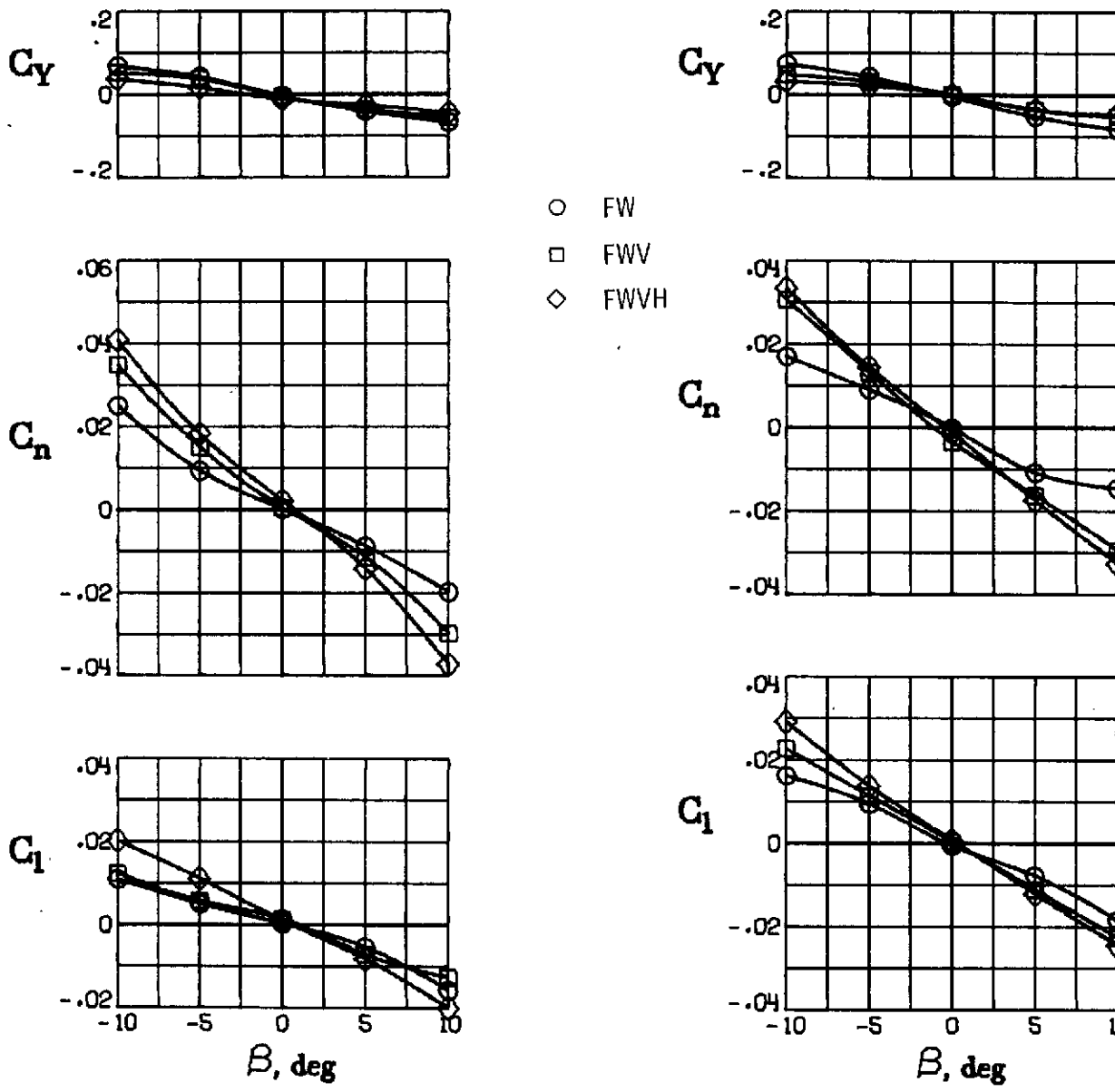

(g) $\alpha = 30^{\circ}$.

(h) $\alpha = 35^{\circ}$.

Figure 5.- Continued.

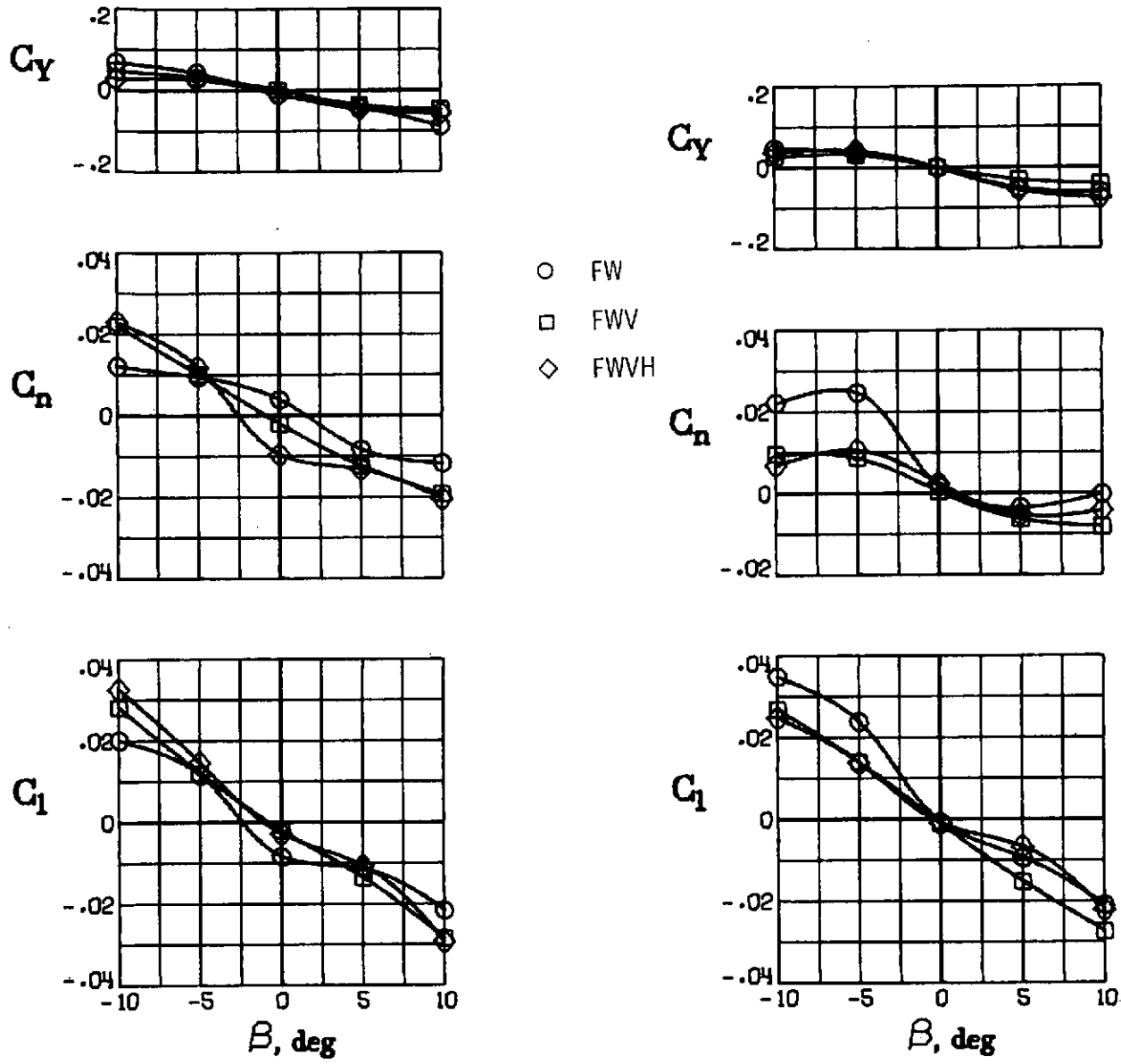

(i) $\alpha = 40^{\circ}$.

(j) $\alpha = 45^{\circ}$.

Figure 5.- Concluded.

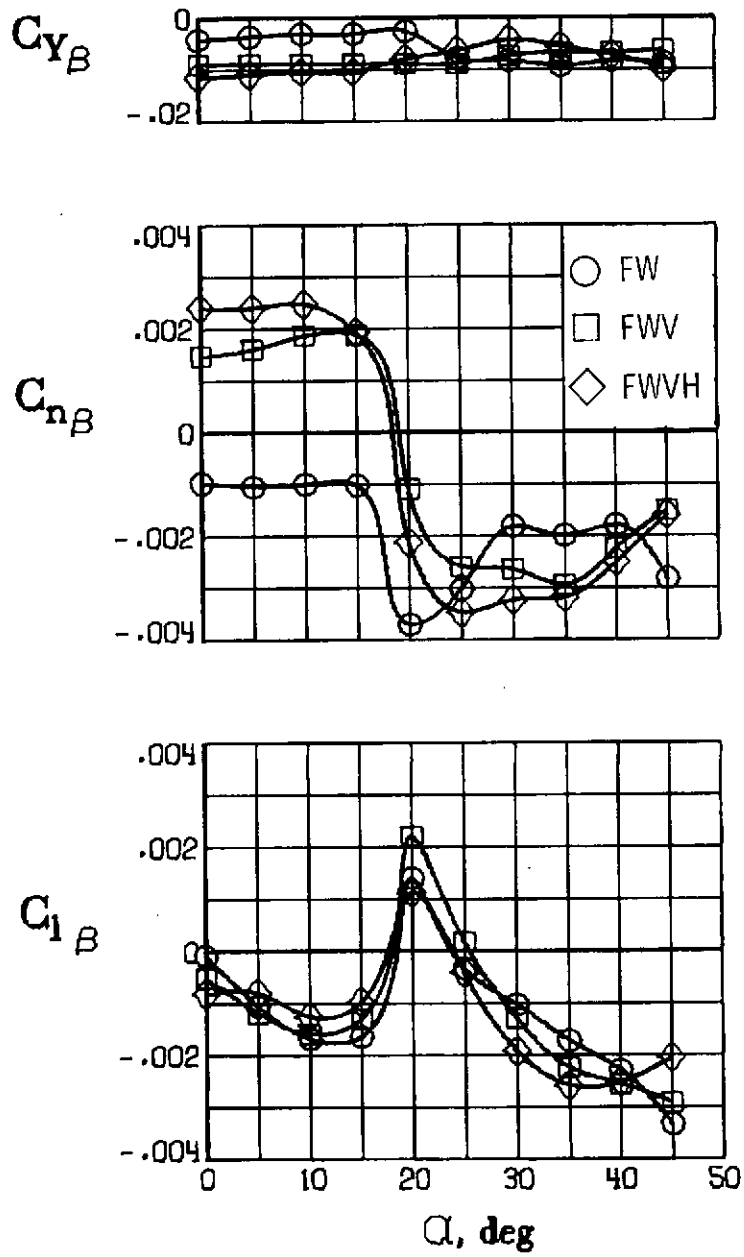

(a) Component buildup study.

Figure 6.- Variation of static lateral-directional stability derivatives with angle of attack.

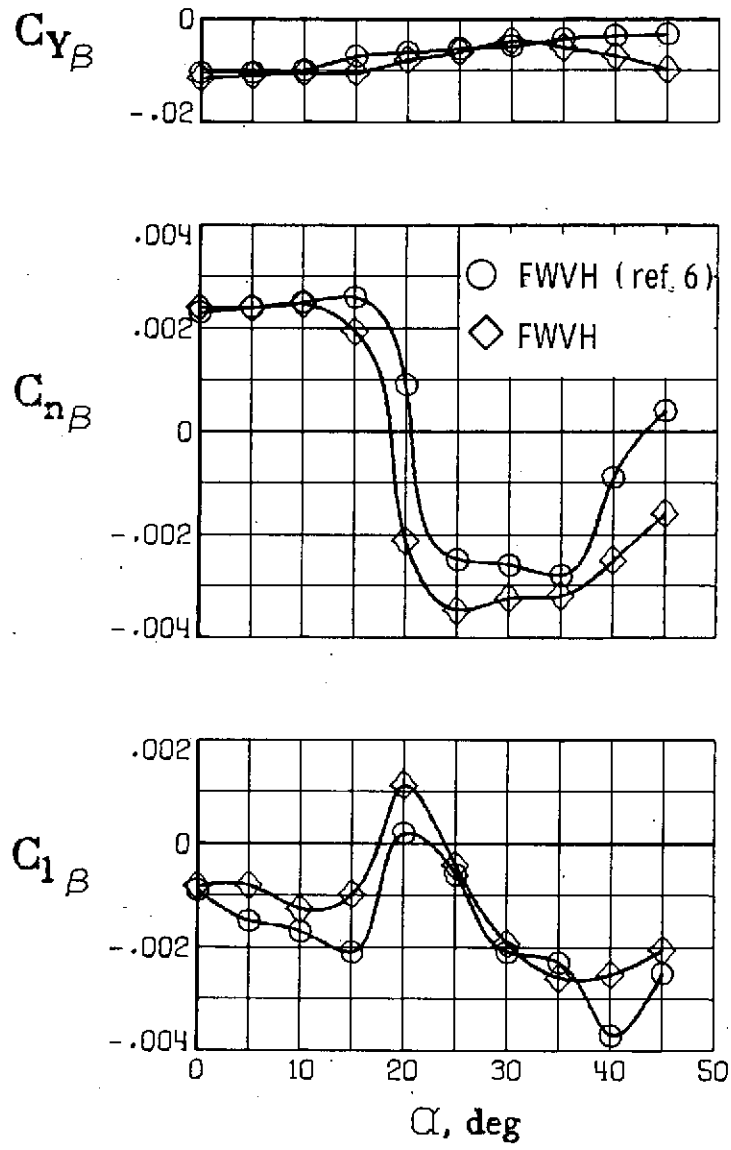

(b) Comparison of static lateral-directional stability derivatives of present investigation with those of reference 6.

Figure 6.- Concluded.

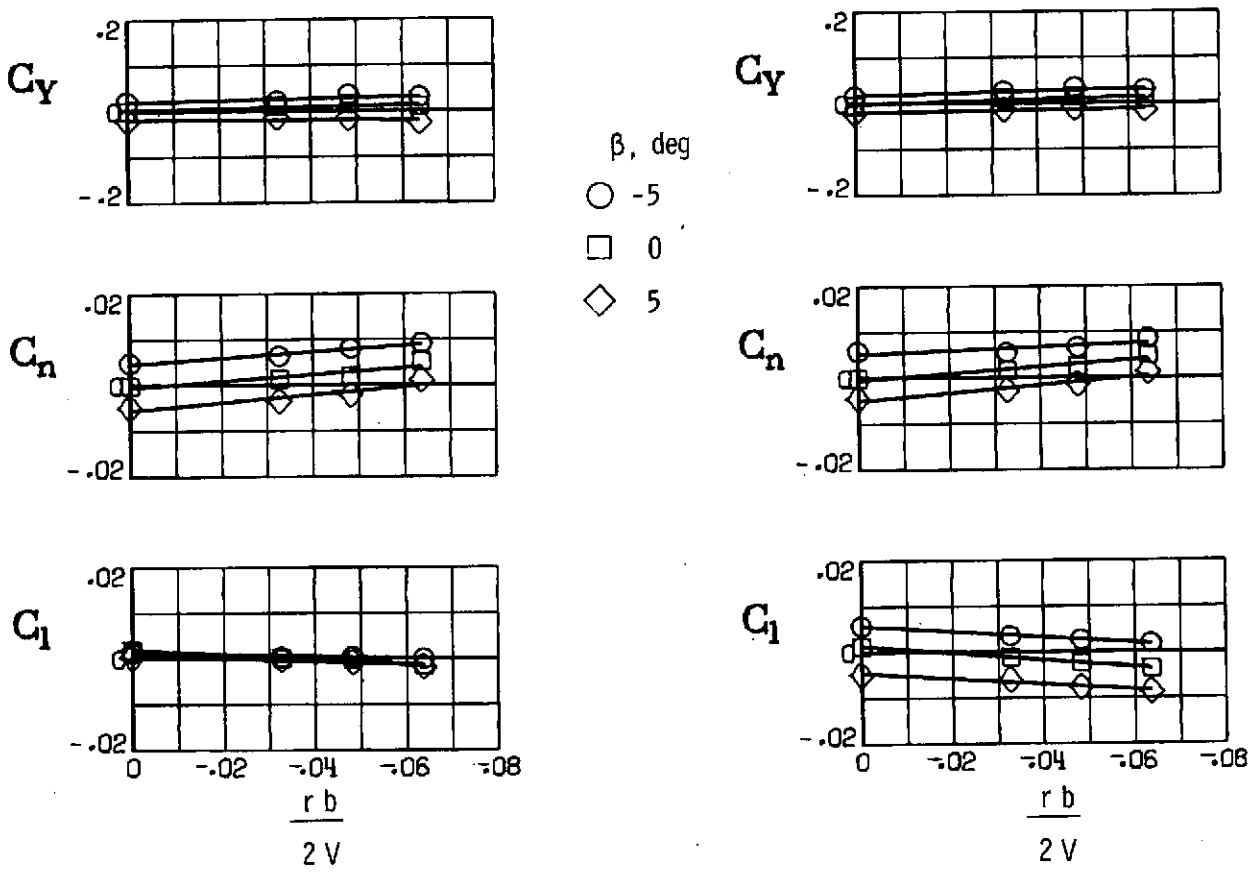

(a) $\alpha = 0^{\circ}$.

(b) $\alpha = 5^{\circ}$.

Figure 7.- Variation of static lateral-directional characteristics with yawing velocity for fuselage-wing combination.

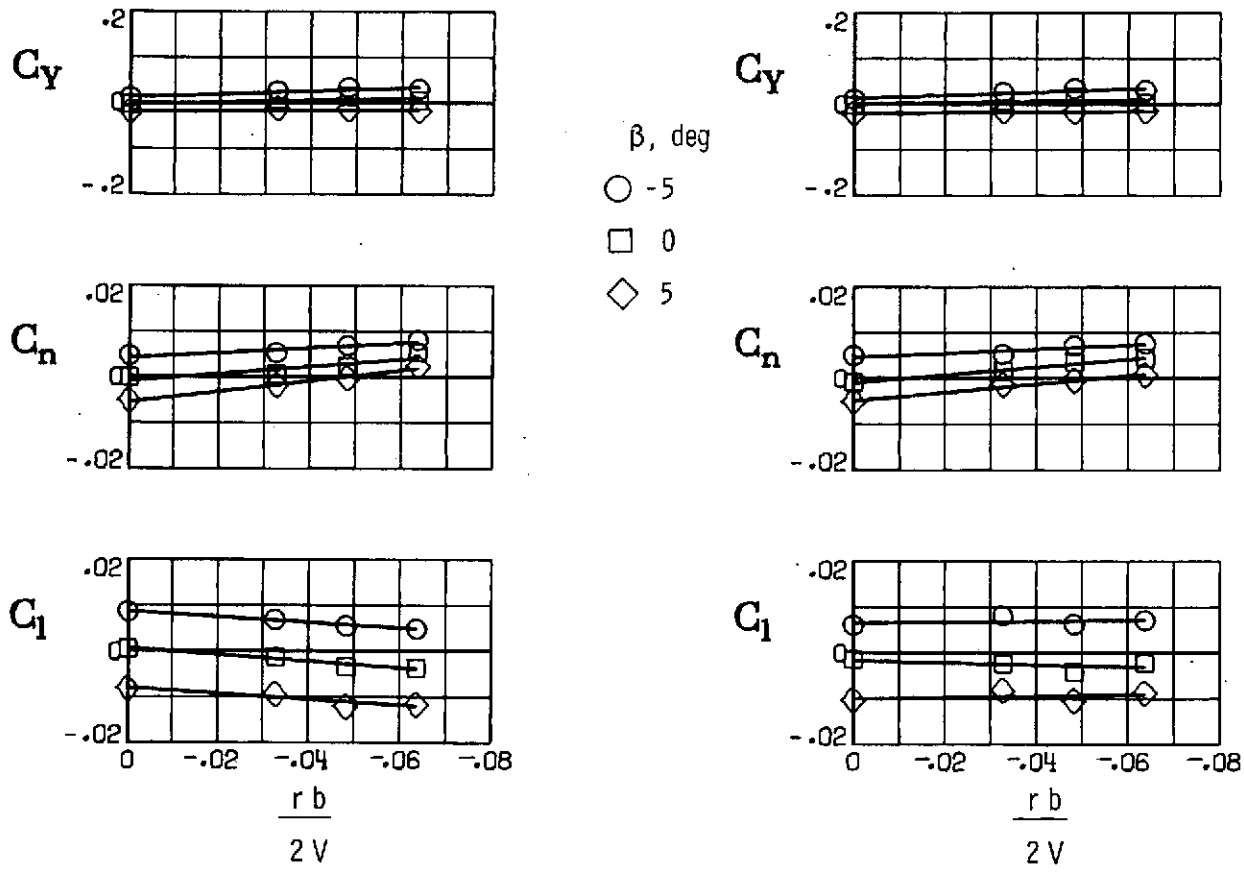

(c) $\alpha = 10^{\circ}$.

(d) $\alpha = 15^{\circ}$.

Figure 7.- Continued.

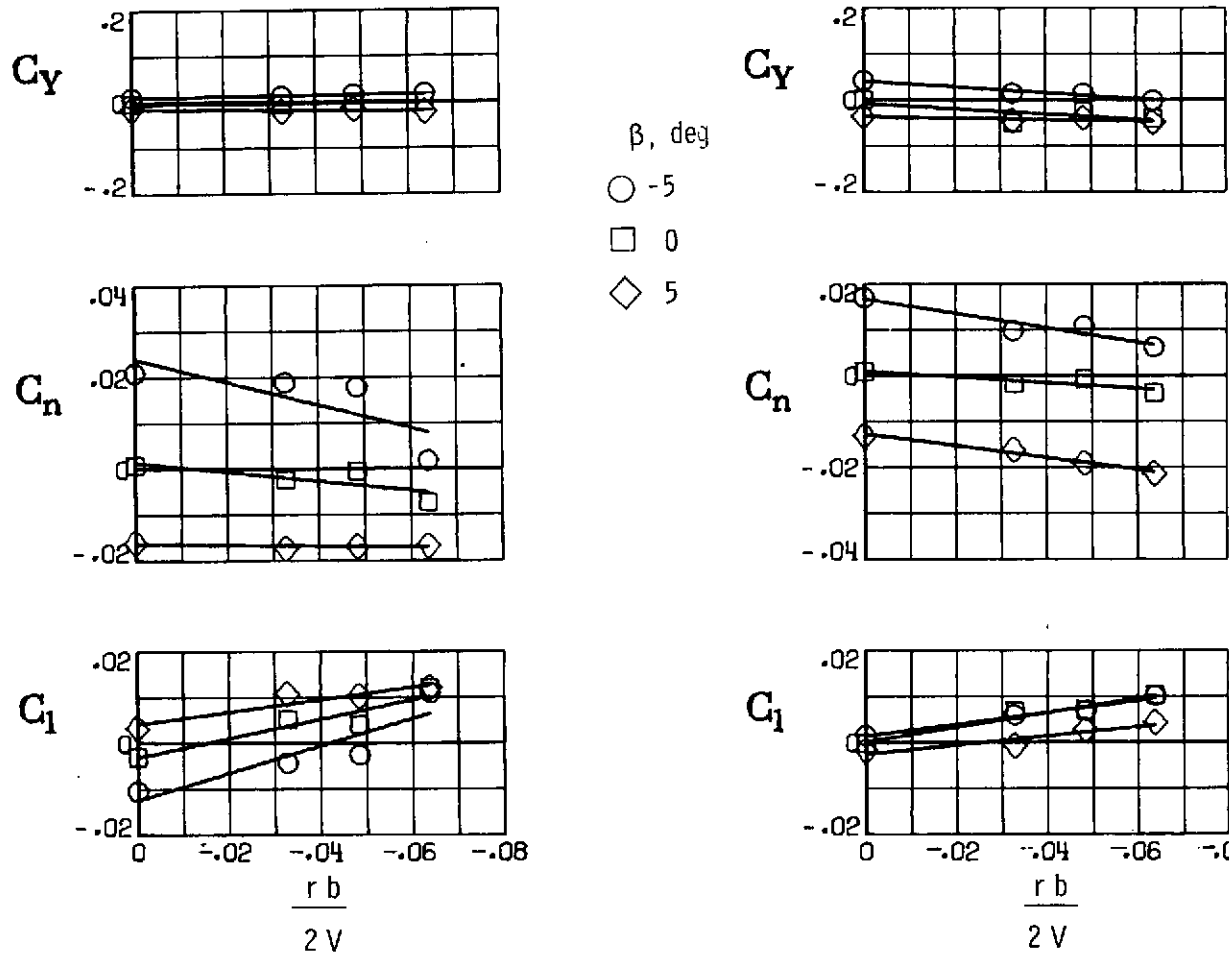

(e) $\alpha = 20^{\circ}$.

(f) $\alpha = 25^{\circ}$.

Figure 7.- Continued.

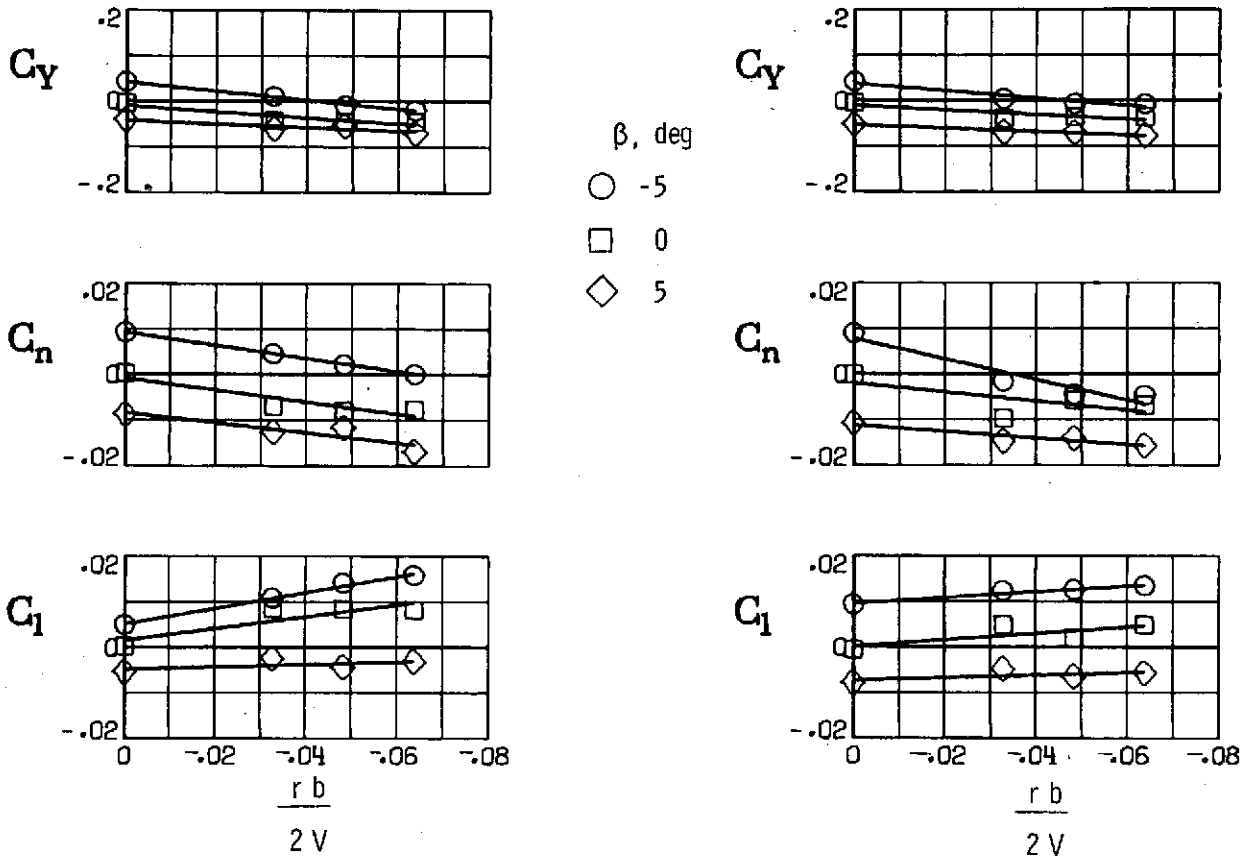

(g) $\alpha = 30^{\circ}$.

(h) $\alpha = 35^{\circ}$.

Figure 7.- Continued.

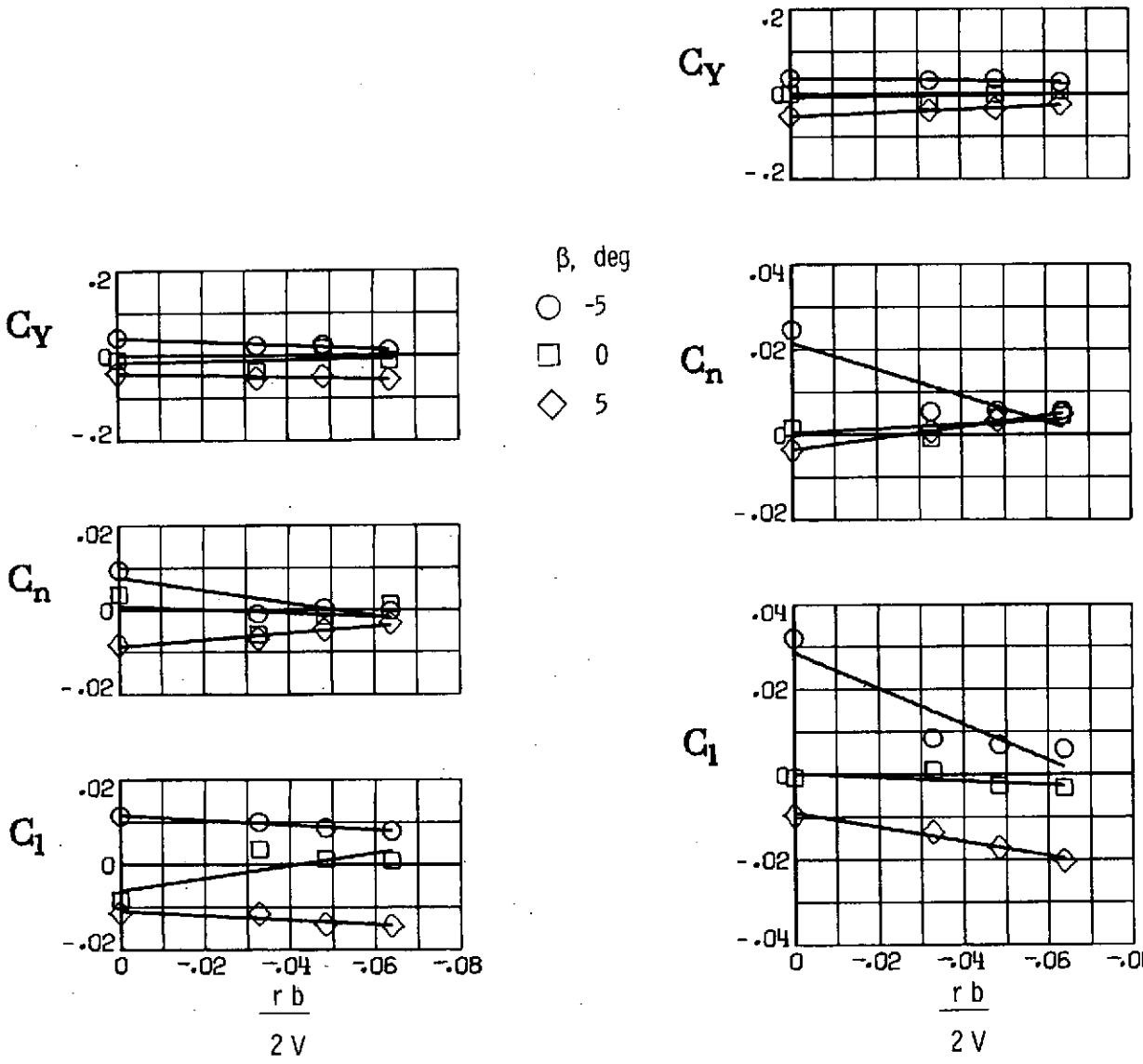

(i) $\alpha = 40^{\circ}$.

(j) $\alpha = 45^{\circ}$.

Figure 7.- Concluded.

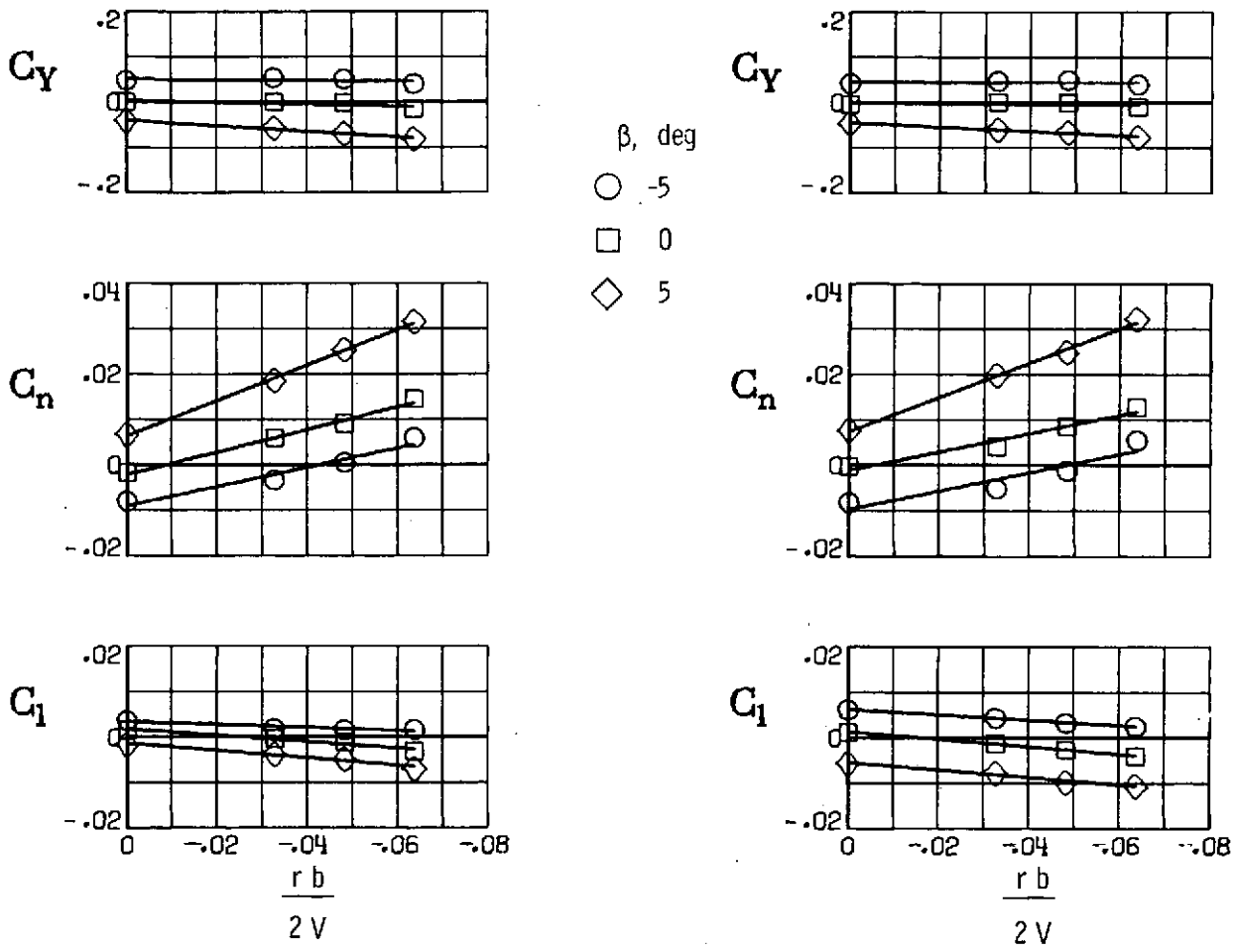

(a) $\alpha = 0^{\circ}$.

(b) $\alpha = 5^{\circ}$.

Figure 8.- Variation of static lateral-directional characteristics with yawing velocity for fuselage-wing—vertical-tail combination.

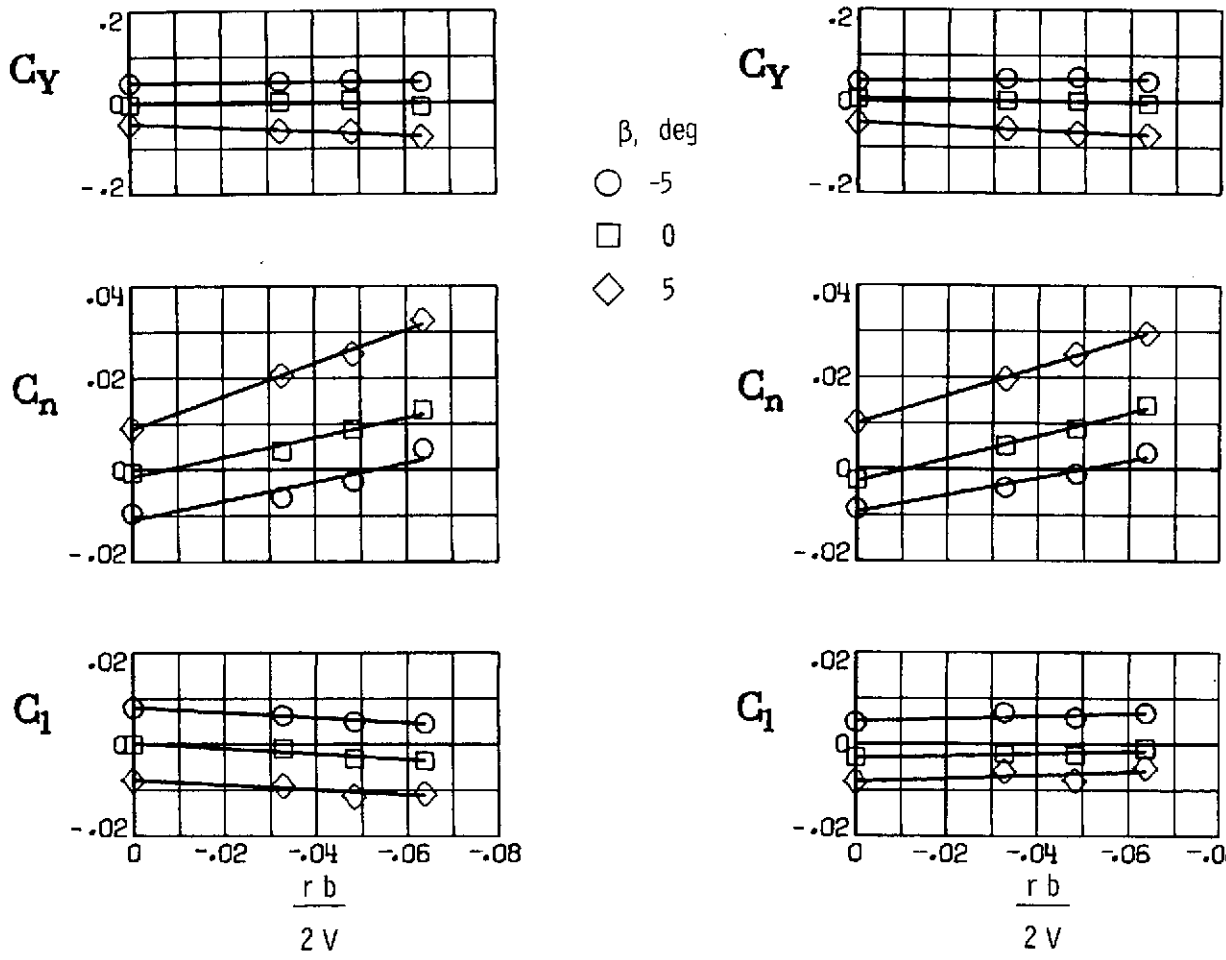

(c) $\alpha = 10^{\circ}$.

(d) $\alpha = 15^{\circ}$.

Figure 8.- Continued.

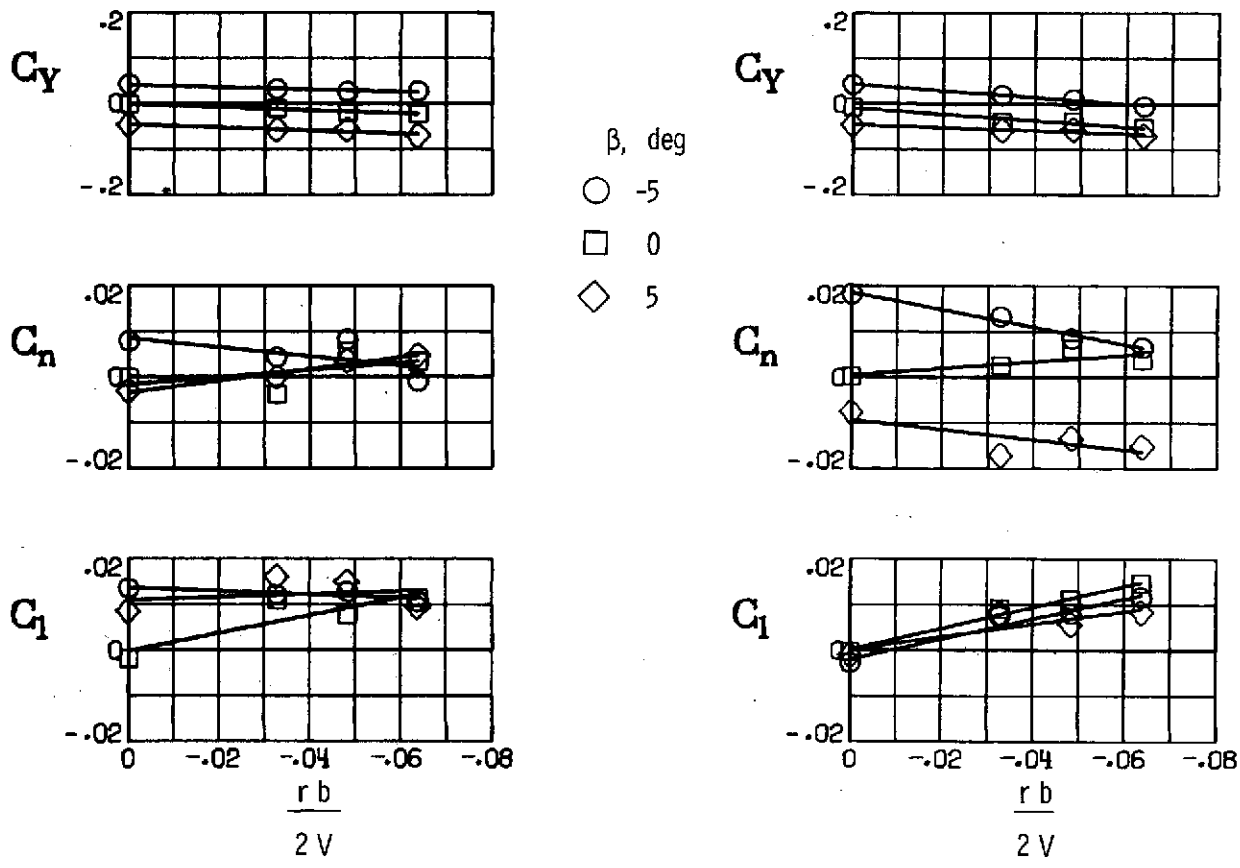

(e) $\alpha = 20^{\circ}$.

(f) $\alpha = 25^{\circ}$.

Figure 8.- Continued.

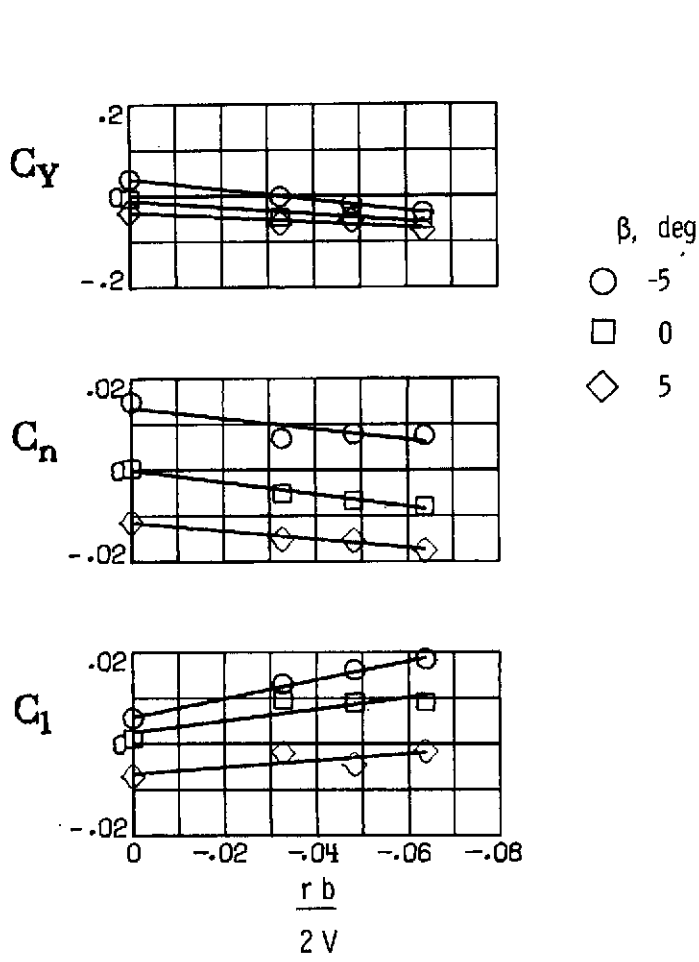

(g) $\alpha = 30^{\circ}$.

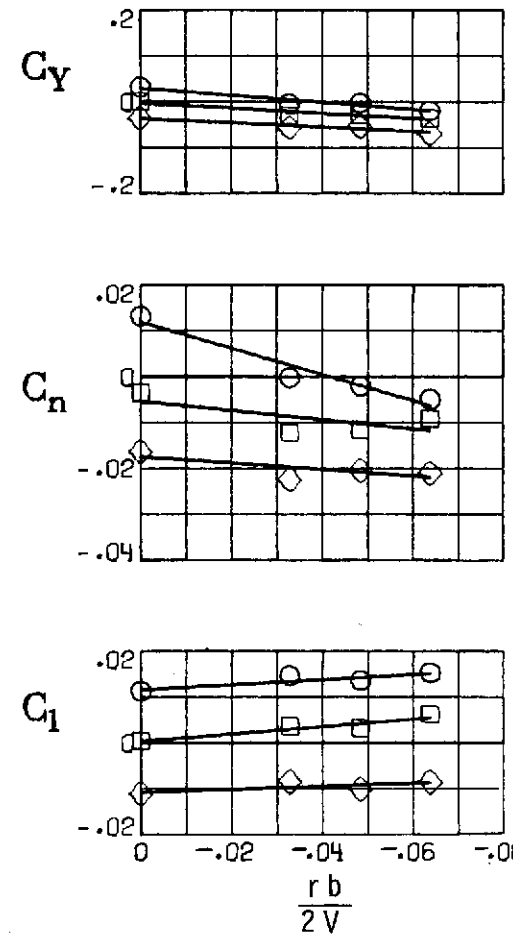

(h) $\alpha = 35^{\circ}$.

Figure 8.- Continued.

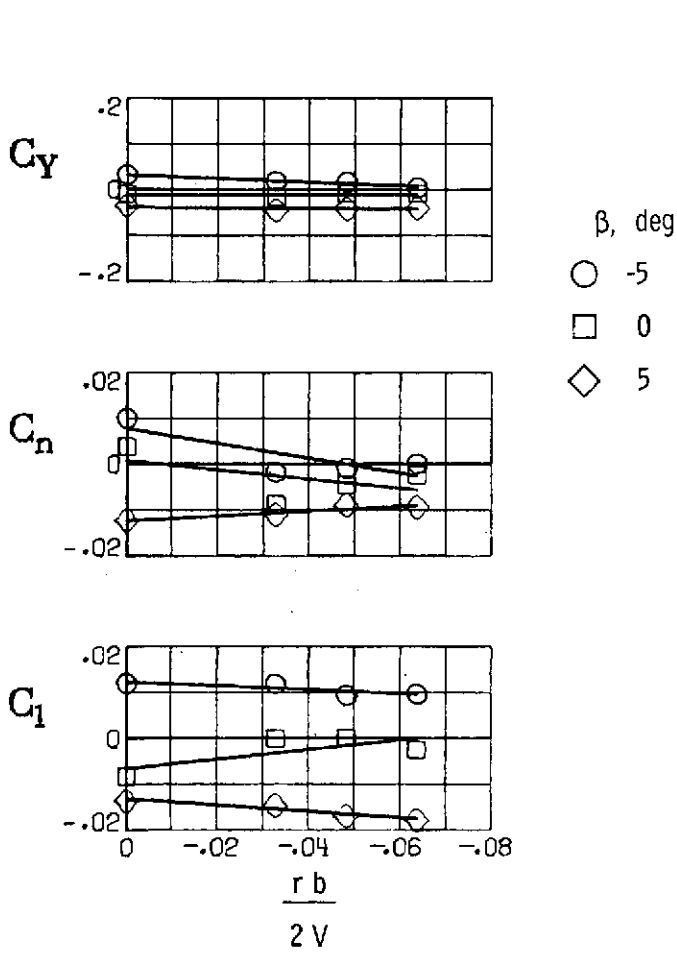

(i) $\alpha = 40^{\circ}$.

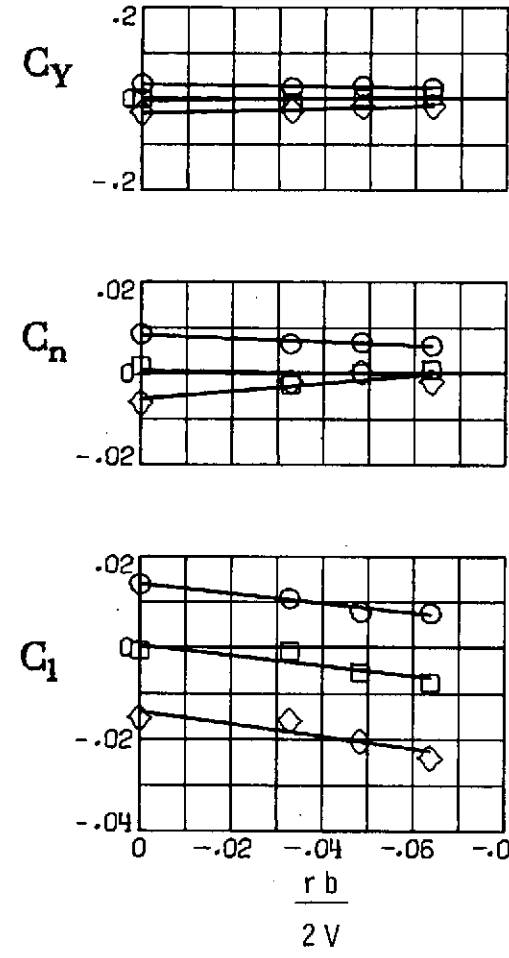

(j) $\alpha = 45^{\circ}$.

Figure 8.- Concluded.

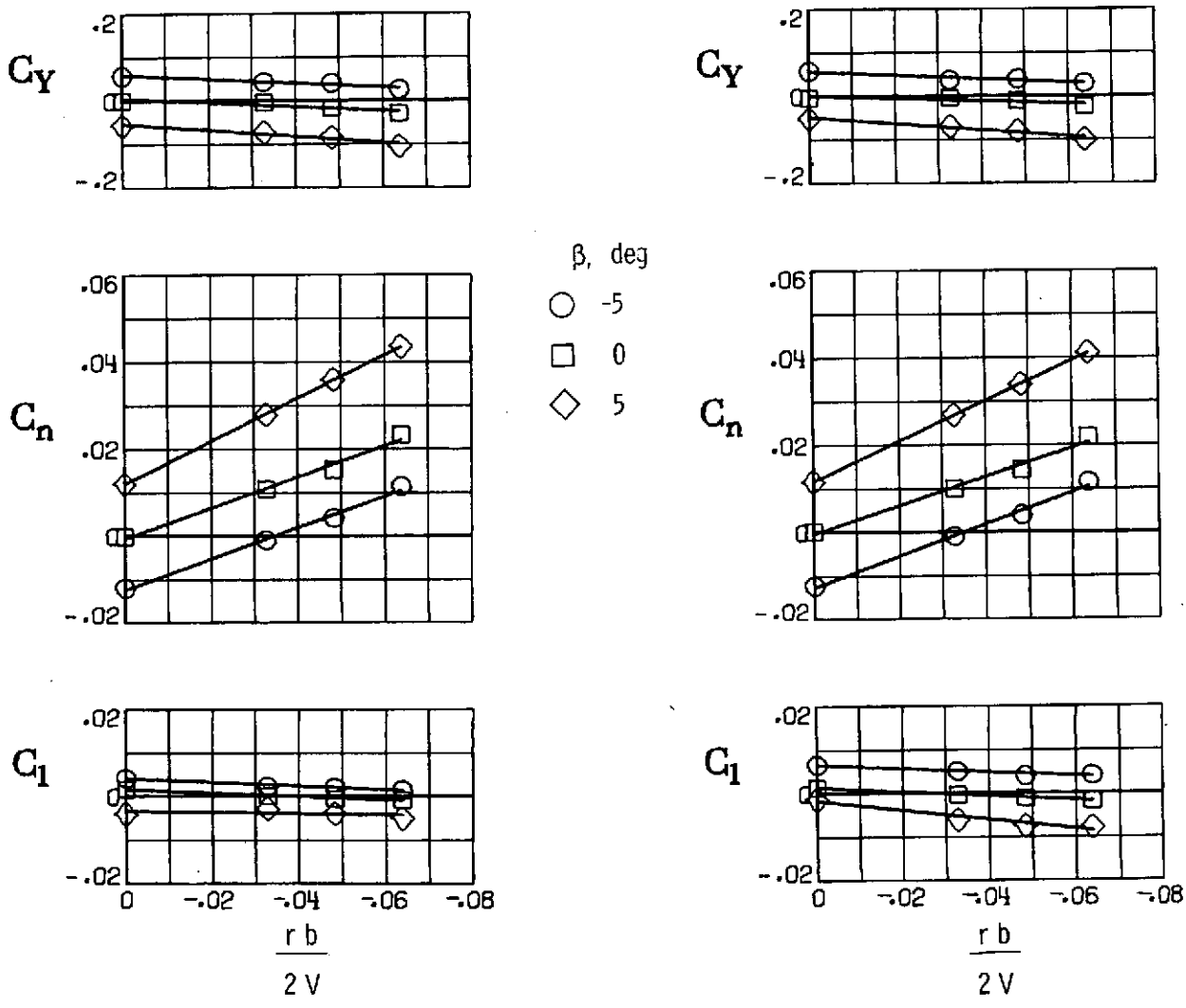

(a) $\alpha = 0^{\circ}$.

(b) $\alpha = 5^{\circ}$.

Figure 9.- Variation of static lateral-directional characteristics with yawing velocity for complete configuration.

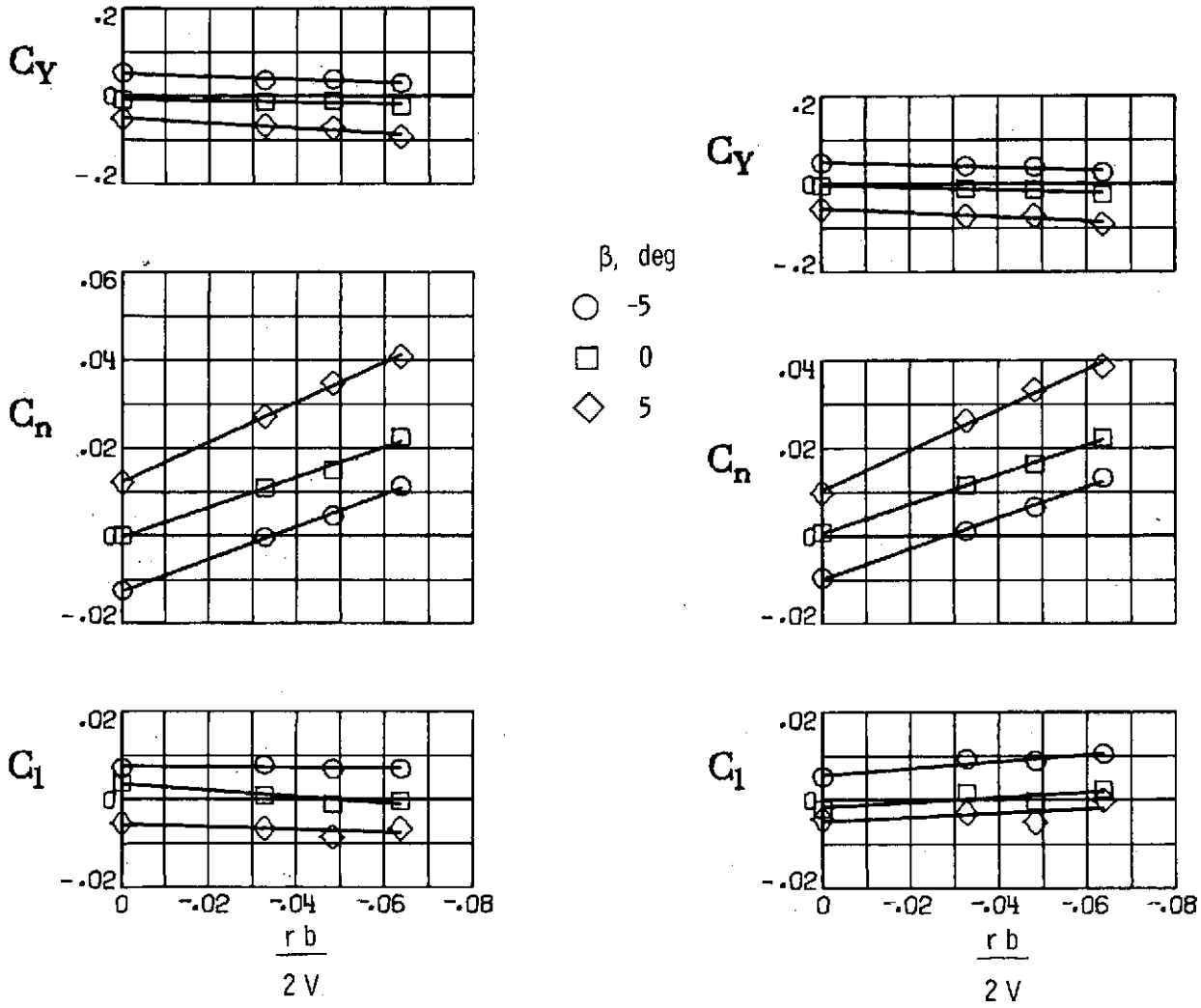

(c) $\alpha = 10^{\circ}$.

(d) $\alpha = 15^{\circ}$.

Figure 9.- Continued.

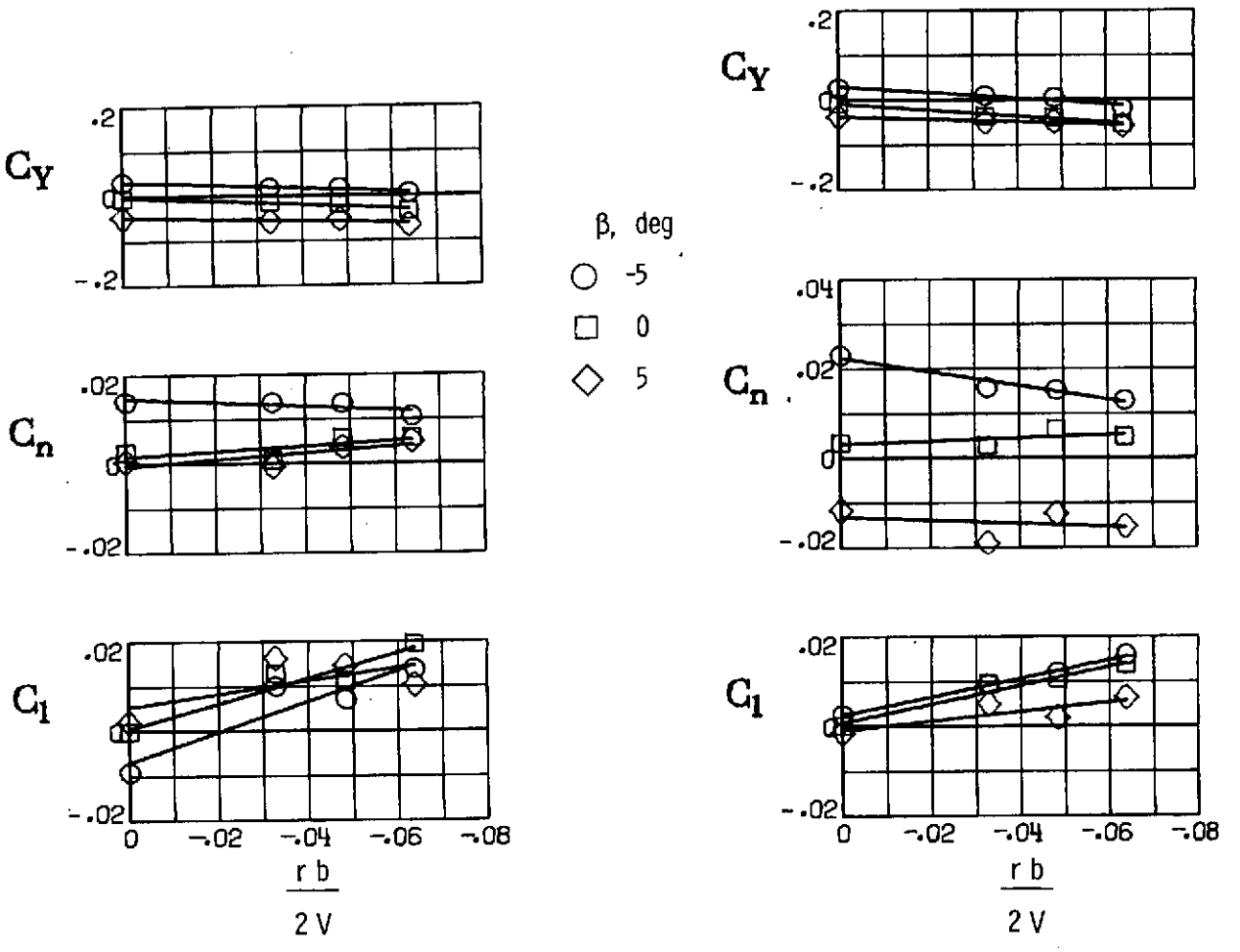

(e) $\alpha = 20^{\circ}$.

(f) $\alpha = 25^{\circ}$.

Figure 9.- Continued.

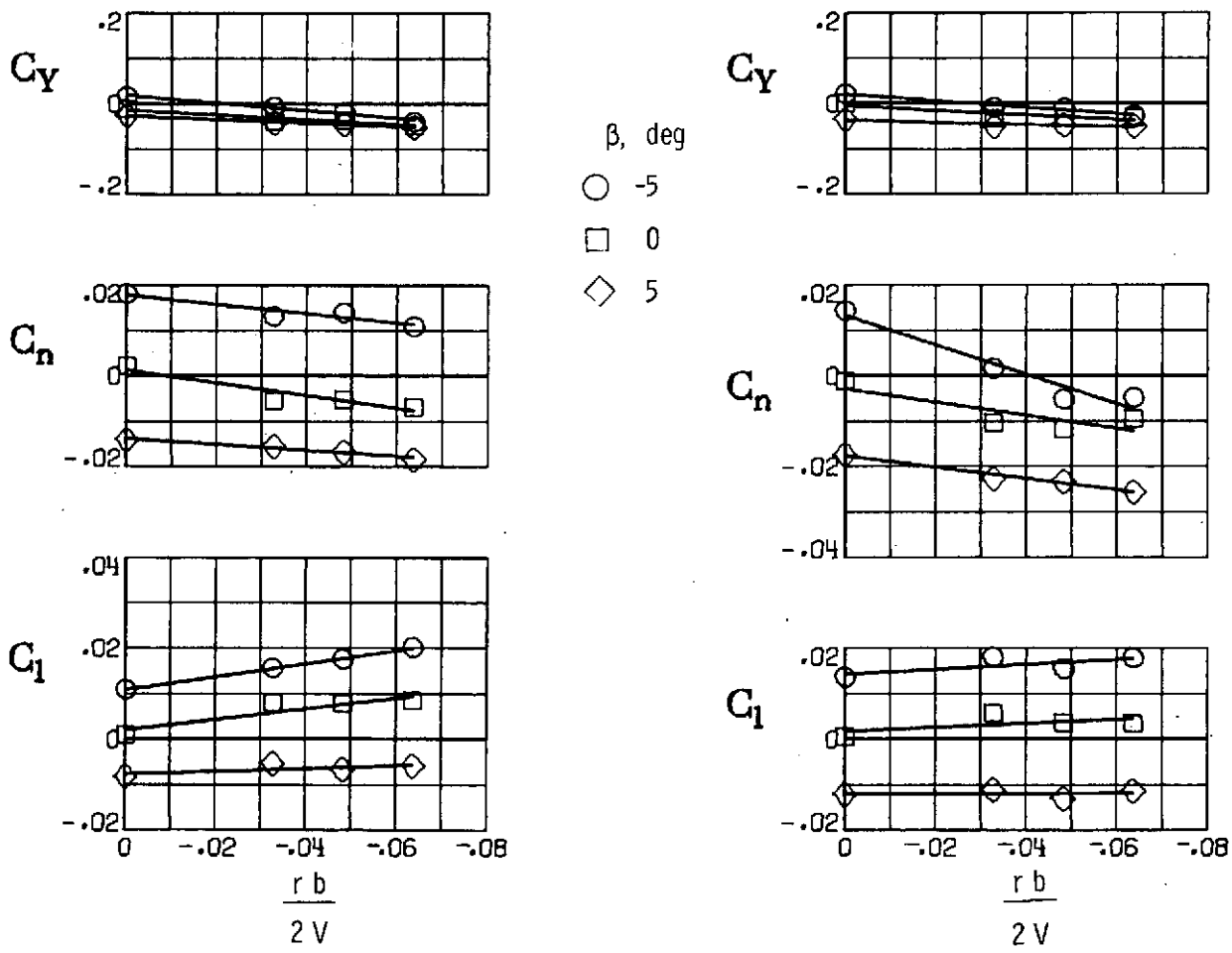

(g) $\alpha = 30^{\circ}$.

(h) $\alpha = 35^{\circ}$.

Figure 9.- Continued.

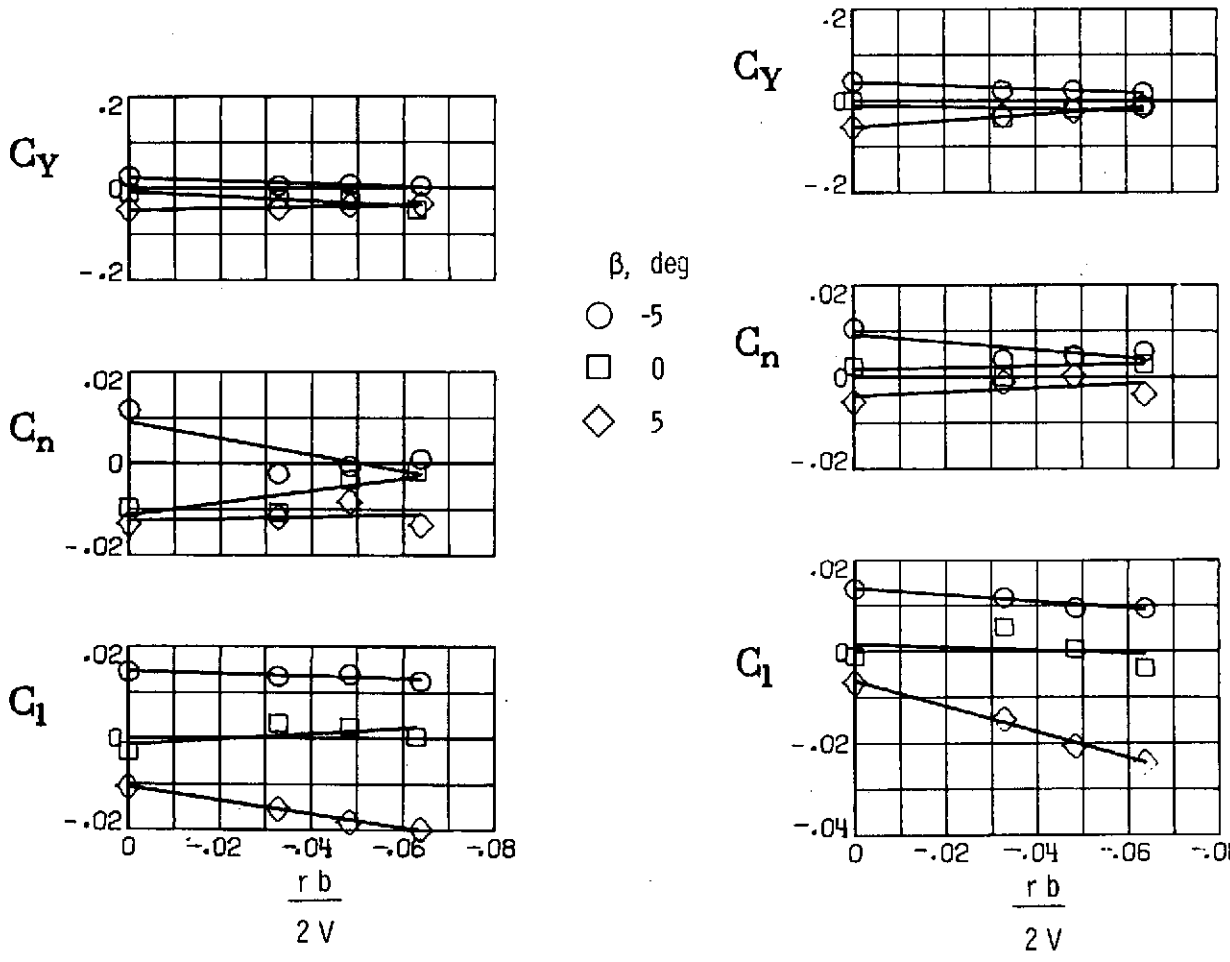

(i) $\alpha = 40^{\circ}$.

(j) $\alpha = 45^{\circ}$.

Figure 9.- Concluded.

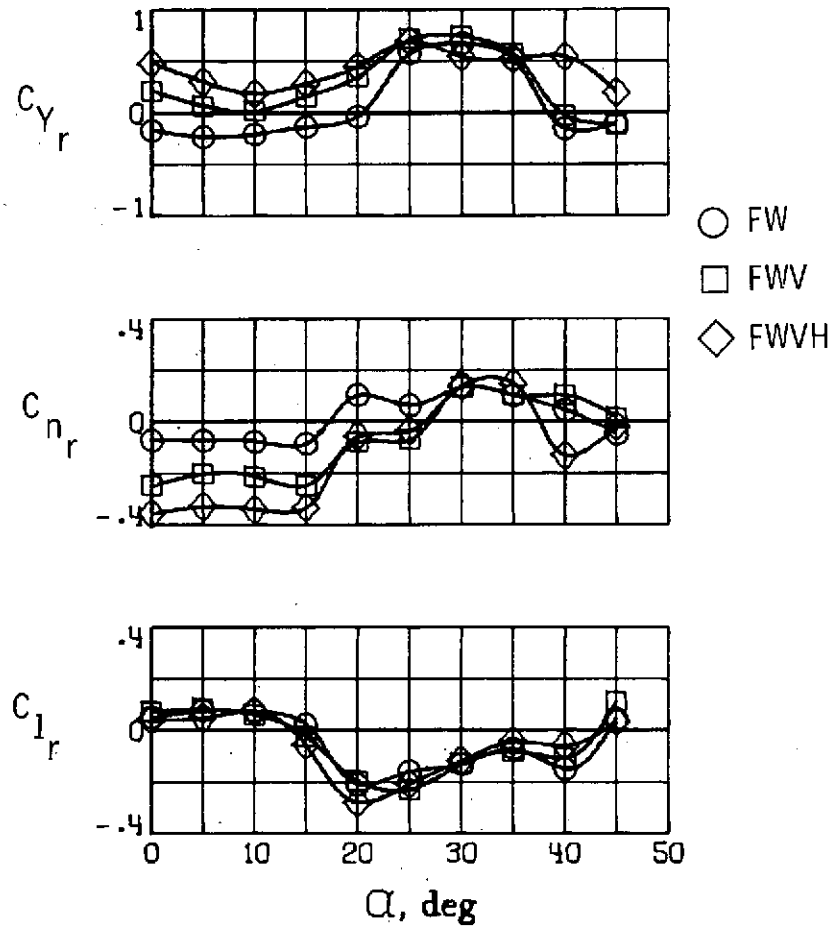

Figure 10.- Variation of yawing stability derivatives with angle of attack for component buildup study. $\beta = 0^{o}$.

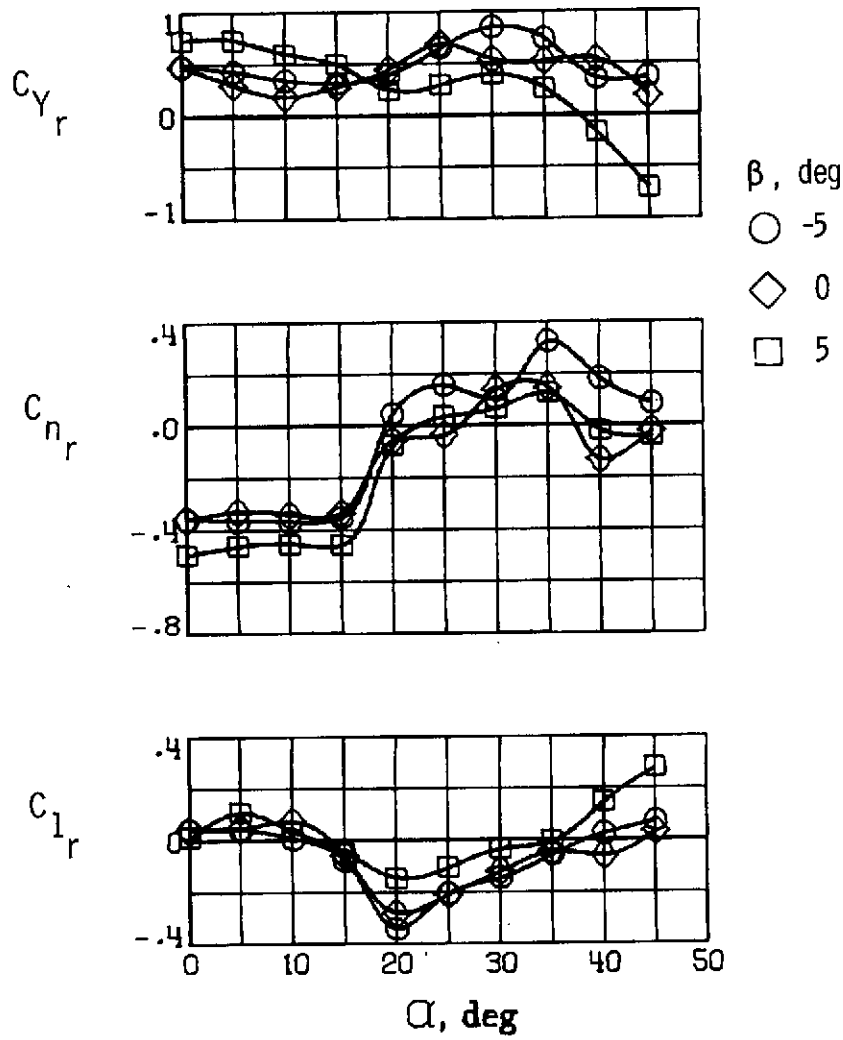

Figure 11.- Variation of yawing stability derivatives with angle of attack and angle of sideslip for complete configuration.

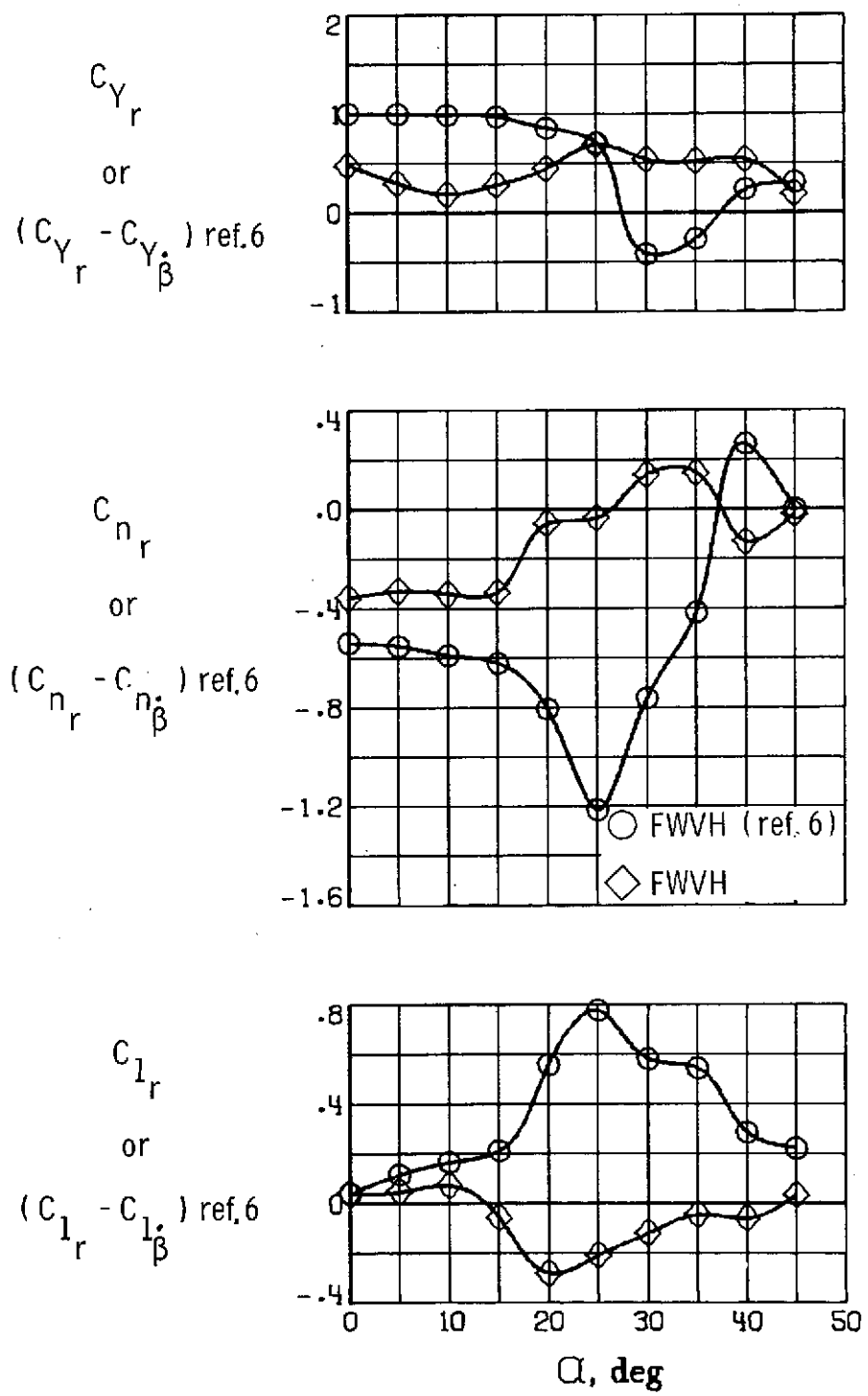

Figure 12.- Comparison of yawing stability derivatives for present investigation with those of reference 6. $\beta = 0^{\circ}$.